REDUCTION OF DRAG OF A SUBMERGED SWIMMER USING VORTEX GENERATORS

By

John Waring

B.A.Sc. (Mechanical Engineering)

A thesis submitted to the Faculty of Graduate Studies and Research in partial fulfilment of the requirements for the degree of

Master of Engineering in Aerospace Engineering

Ottawa-Carleton Institute for Mechanical and Aerospace Engineering

Department of Mechanical and Aerospace Engineering

Carleton University

Ottawa Ontario

August 1999

© 1999

John Waring

National Library of Canada
Acquisitions and Bibliographic Services
395 Wellington Street
Ottawa ON K1A 0N4
Canada

Bibliothèque nationale du Canada
Acquisitions et services bibliographiques
395, rue Wellington
Ottawa ON K1A 0N4
Canada

Your file Votre référence

Our file Notre référence

The author has granted a non-exclusive licence allowing the National Library of Canada to reproduce, loan, distribute or sell copies of this thesis in microform, paper or electronic formats.

L'auteur a accordé une licence non exclusive permettant à la Bibliothèque nationale du Canada de reproduire, prêter, distribuer ou vendre des copies de cette thèse sous la forme de microfiche/film, de reproduction sur papier ou sur format électronique.

The author retains ownership of the copyright in this thesis. Neither the thesis nor substantial extracts from it may be printed or otherwise reproduced without the author's permission.

L'auteur conserve la propriété du droit d'auteur qui protège cette thèse. Ni la thèse ni des extraits substantiels de celle-ci ne doivent être imprimés ou autrement reproduits sans son autorisation.

0-612-48464-5

Canada

ABSTRACT

Regions of separated flow constitute a significant source of drag for competitive swimmers particularly during the submerged portions of the race, which occur immediately after each start and turn. Since races are frequently decided by fractions of a second, even modest drag reductions could have a significant effect on the outcome of a competition.

The author has proposed the use of vortex generators to minimize separation bubbles thereby reducing overall swimmer drag. The purpose of this research project was to determine the optimal type, size and arrangement of vortex generators to minimize overall drag.

To this end, drag measurements of a one half-scale model of a swimmer with various vortex generators were taken in Carleton University's closed-circuit low-speed wind tunnel. The results suggest that vortex generators could reduce the drag coefficient for a submerged swimmer by as much as six percent. The minimum drag for a practical configuration was achieved with a double inline row of Kuethe type vortex generators of approximately one-tenth inch scale height (one twentieth of an inch on the model).

This configuration was incorporated into a swimsuit worn by American swimmers at the 1996 Atlanta Olympic games (Jenny Thompson won three relay gold medals) and the 1998 World Championships in Perth Australia (various medals and records).

ACKNOWLEDGEMENTS

Dr. Steen Sjolander provided clear advice and exhibited profound patience as I juggled this thesis with business commitments.

Dr. Tom Currie provided detailed insight into the advantages and perils of experimental versus computational approaches to fluid mechanics.

In addition to his testing advice, Ross Cowie's surfboard making expertise proved critical in constructing the wind tunnel model.

Dr. Mike Benner provided numerous testing suggestions.

Mr. Stu Isaac, Vice President of Authentic Fitness Corporation (Speedo America), shared his considerable swimsuit testing experience and invited me to attend test sessions at the International Centre for Aquatic Research (ICAR). In addition, Speedo America provided financial support.

Finally, I thank the faculty and staff of Carleton University for their unending patience with me.

TABLE OF CONTENTS

LIST OF TABLES

LIST OF FIGURES

1 INTRODUCTION

The margin of victory in competitive swimming is often measured in hundredths of seconds. Consequently, even a modest reduction swimmer drag would be significant to the competitor. Although skin friction is the least significant form of drag for the human swimmer, it has been the focus of most drag reduction efforts to date. Commonly, competitors will shave most of their body hair to reduce skin friction for major competitions. In addition, manufacturers have developed fabrics that reduce the friction of water flowing over the swimsuit. However, the high drag coefficient for submerged humans suggests that form drag is the dominant mode during the underwater phases of competition.

Various vortex generators have been used in aeronautical and marine applications to delay the boundary layer separation that causes form drag. The author has proposed affixing vortex generators to swimwear at essential locations in order to achieve the same effect for competitive swimmers (Waring, 1998). The goal of the present research was to refine the placement, size, and shape of the vortex generators in order to specify a practical arrangement that will produce the lowest overall drag for a swimmer. After surveying previous swimmer drag measurement methods, the author decided upon wind tunnel testing primarily for reasons of repeatability and rapid turn-around between tests.

Computer simulation employing computational fluid dynamics (CFD) was initially considered for its excellent repeatability and flow visualization. However, this approach had several shortcomings that made it impractical at the time this thesis was being planned. The fine mesh, needed to resolve both the vortices and the swimmer's various separation bubbles, would have required prohibitive modelling time. In addition, the computational power required to calculate such a mesh was not readily available.

The optimization testing was conducted in Carleton University's low-speed closed-circuit wind tunnel. The test article was a half scale fibreglass model of a swimmer in the 'streamlined position' (hands overlapping with arms extended over the head). This configuration allowed repeatable testing at Reynolds numbers within the flow regime of competitive swimming. The swimmer model provided a reasonably anthropomorphic test article without the inherent variability of a live test subject.

Testing focused on two types of vortex generators, Stephens (1957) and Kuethe (1970). While the Stephens type did yield promising results in the wind tunnel, it proved impractical when scaled up and attached to actual swimwear. The Kuethe type ultimately proved to be more practical and was highly successful in competition.

The test results are applicable to the submerged portions of the race. While results from competition tend to support the wind tunnel test results, a more comprehensive in-water, live-swimmer test program is recommended to confirm this finding.

2 BACKGROUND

2.1 Swimmer Drag

2.1.1 Humans and Cetaceans

The human body is poorly shaped for aqueous locomotion in comparison with aquatic mammals. Currently, the 'fastest man afloat' is Tom Jager who has achieved an average velocity of 8.64 km/hr over 50yds (Wyse, 1997). This however compares poorly with observed speeds for the Dall's Porpoise of 55.4 km/hr (Wyse). This large disparity is at least in part attributable to differences in the drag coefficient. Using the greatest cross-sectional area as a reference, Clarys (1978) estimated the drag coefficient for a submerged swimmer as being between 0.58 and 1.04. Gross et al (1983) estimated the drag coefficient of a prone cyclist in air at 0.6 (not including the bicycle). By comparison, Tietjens (1957), Landolt and Börnstein (1955), and McNeill (1968) estimated the drag coefficient of a dolphin as 0.055 to 0.075.

2.1.2 Drag Sources for a Swimmer

2.1.2.1 Skin Friction

Skin friction is the dominant source of drag for streamlined bodies such as dolphins. The order-of-magnitude higher drag coefficient for a human strongly suggests that skin friction is not the dominant source of drag for a swimmer. Despite this, skin friction in competitive swimming, until recently, has been the focus of most efforts to reduce drag.

2.1.2.2 Wave Drag

When moving at or near the surface of the water a swimmer generates a series of waves that carry energy away from the swimmer. Competitors avoid this type of drag by remaining submerged after starts and turns as long as the rules will allow. Recently the Federation International de Natation Amateur (FINA), the international governing body for aquatics, amended the rules for freestyle, backstroke and butterfly to prevent athletes from swimming more than 15 metres submerged after each start or turn. Since 1957, breaststroke has been limited to one pull and one

kick underwater after each start or turn. Prior to the changes, several world records were established by competitors who remained submerged for more than half the race distance.

2.1.2.3 Form Drag

For the submerged swimmer, separation bubbles are probably the primary drag source. What competitive swimmers term the 'streamlined' position (arms extended over the head with hands overlapping) is more accurately described as a minimum drag position. The high drag coefficient, even in the streamlined position, strongly suggests that the flow does not follow the contours of the body. Rather, the flow separates in areas of adverse pressure gradient, such as the lower half of the buttocks. Along the swimmer's back, numerous contours create adverse pressure gradients resulting in large separation bubbles. These were clearly observed by the author during flume testing of swimmers at the International Centre for Aquatic Research (ICAR) in Colorado Springs. The flowing water contained a large number of small air bubbles that provided flow visualisation. As anticipated, there was a large separation bubble behind the buttocks. In addition, there was also a separation bubble in the small of the back. These are shown schematically in figure 2.1.

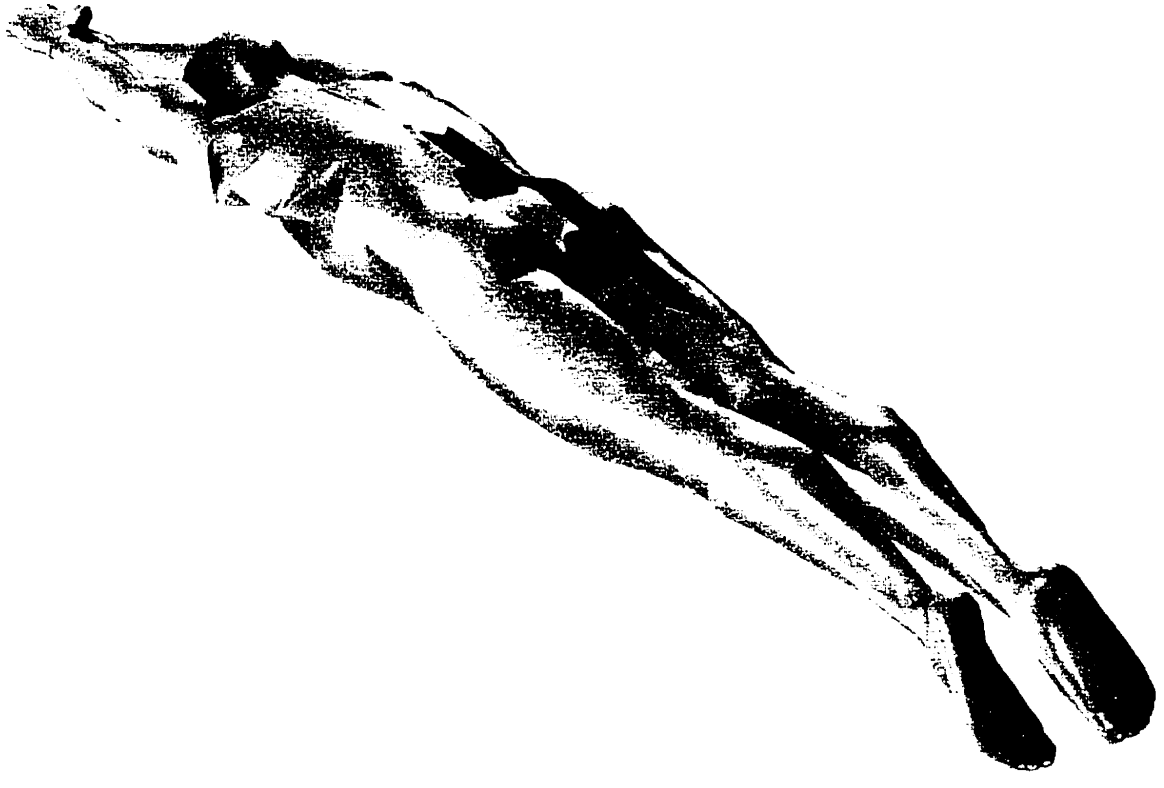

Figure 2.1: Separation Bubbles for Prone Swimmer

2.1.3 Classic Drag Reduction Techniques

2.1.3.1 Shaving Body Hair

Swimming is becoming increasingly competitive with races frequently decided by tenths of seconds or less. Consequently, even minimal drag reduction can have a significant effect on the outcome of a race. This is evidenced by the widespread practice of 'shaving down' prior to major competitions. This involves shaving most of the body (sometimes including the head and eyebrows) to achieve a more hydrodynamically smooth surface.

2.1.3.2 Tight Suit

Wearing a tightly fitting swimsuit has several advantages, particularly for women. The suit tends to flatten out the contours of the body and reduce the amount of water that flows between the suit and the skin surface thereby reducing form drag. In addition, Kraemer et al (1996) showed that fabric compression around muscles would reduce muscular vibration and thereby reduce fatigue.

2.1.4 Other Developments in Suit Design

2.1.4.1 Denser weave

Competitive swimsuit manufacturers, until recently, have focused on reducing the skin friction of the fabric. This generally involves increasing the stitch density of the knit or weave to reduce porosity and decrease surface roughness. However, despite the best efforts of swimsuit manufacturers, a practical suit has not yet been designed which completely prevents water from flowing into the space between the fabric and the skin. Consequently, the suit material must maintain some minimum porosity in order to prevent ballooning and its commensurate drag increase.

2.1.4.2 'Hydrophobic' Materials

Various manufacturers have introduced 'hydrophobic' materials. These fabrics are typically treated with a polymer such as Teflon. Presumably, the polymer molecules gradually shed into the boundary layer thereby increasing the fluid viscosity in the near-wall region and reducing shear stress.

2.1.4.3 Longitudinal Riblets

One manufacturer has affixed riblets onto some areas of the suit. Walsh (1980) first suggested riblets as a general means of turbulent skin friction reduction. If, however, skin friction accounts for only a small fraction of the total drag on a swimmer, then greater overall improvements may be possible by focusing on more dominant drag sources such as form drag.

2.1.4.4 Serendipitously Located Seams

In the process of constructing a swimsuit, various pieces of fabric must be stitched together. Although manufacturers attempt to minimize the height of these seams, they nonetheless form a significant boundary layer obstacle. When these seams are located on the upstream (near the head) portion of the suit, they may trip the boundary layer into turbulence. This will tend to delay separation in regions of high adverse pressure gradient.

2.1.4.5 Bump Arrays

Some competition suits incorporate an array of small bumps on the chest area. This is has the effect of tripping the boundary layer to delay separation aft of the chest. However, no separation was observed in the chest area when testing swimmers in a flume at the International Centre for Aquatic Research (ICAR) in Colorado. The tightness of the suits normally worn by competitive swimmers tends both to flatten the soft tissues of the chest while smoothly stretching out over gaps. The result is diminishment of the adverse pressure gradient downstream of the chest and a reduced tendency for the flow to separate even without boundary layer energization.

2.1.5 Vortex Generators

2.1.5.1 General Principles of Operation

Vortex generators are generally employed to prevent or delay boundary layer separation in areas of high adverse pressure gradient. Typically, vortex generators are installed in a row across the body upstream of the adverse pressure gradient. This creates a series of closely spaced vortices that persist through the region of adverse pressure gradient. These vortices mix the high-speed free-stream flow away from the body with the low-speed flow in the boundary layer. The

resulting rise in wall shear stress delays the onset of flow separation. Classically, the height of the vortex generator is 0.5 to 1.5 times the boundary layer thickness (Kuethe and Chow, 1986).

2.1.5.2 Types of Vortex Generators

Figure 2.2 shows vortices being generated downstream of vane type vortex generators. These are the most commonly seen and typically consist of rectangular or triangular plates mounted perpendicularly to the surface and canted to the flow direction. Despite their simplicity and widespread usage, the high device drag and requirement for a stiff protrusion make the vane type unsuitable for athletic apparel.

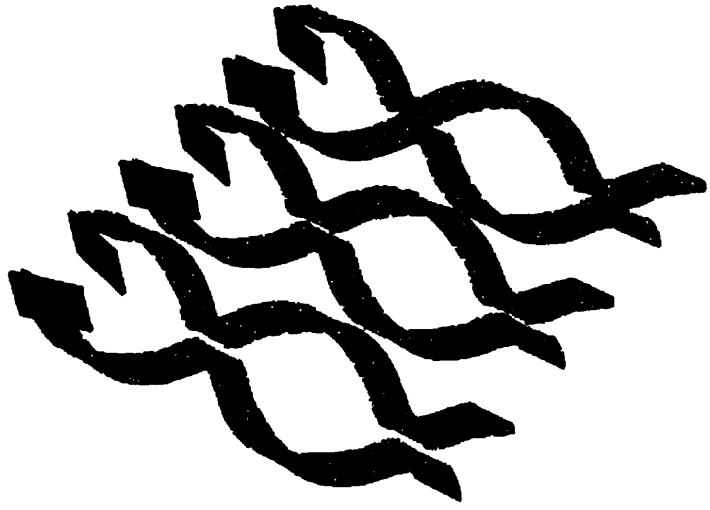

Figure 2.2: Vane Vortex Generators

The Stephens vortex generator, as shown in figure 2.3, was invented based on observations of flow around NACA inlet ducts (Stephens, 1957). Since NACA inlet ducts have been optimized for maximum efficiency, one would expect a lower device drag for the Stephens than the vane type.

The general shape is also better suited to garment attachment. The larger base area makes it easier to bond to fabric. In addition, a Stephens vortex generator can be made from a flexible polymer. This allows the vortex generator to conform to the surface contours when the swimsuit is worn.

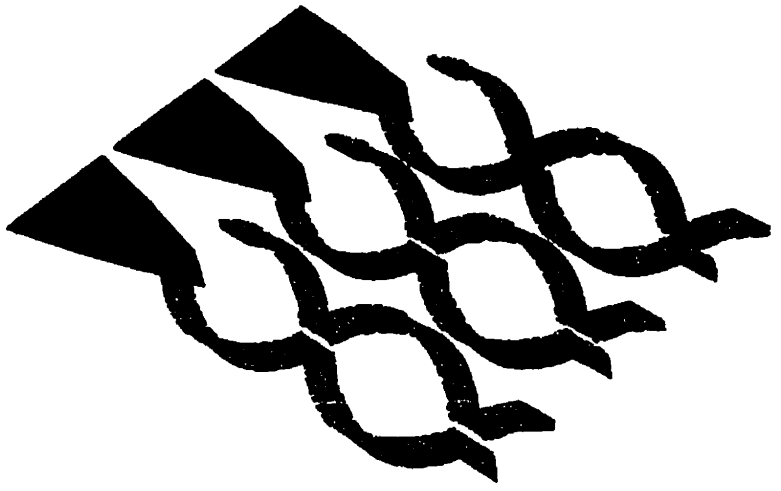

Figure 2.3: Stephens Vortex Generators

Kuethe (1970) first proposed the use of 'V' shaped protrusions, as shown in figure 2.4, for efficient vortex generation. This type ultimately proved to be effective at drag reduction. In addition, they proved to be more durable when incorporated into a swimsuit.

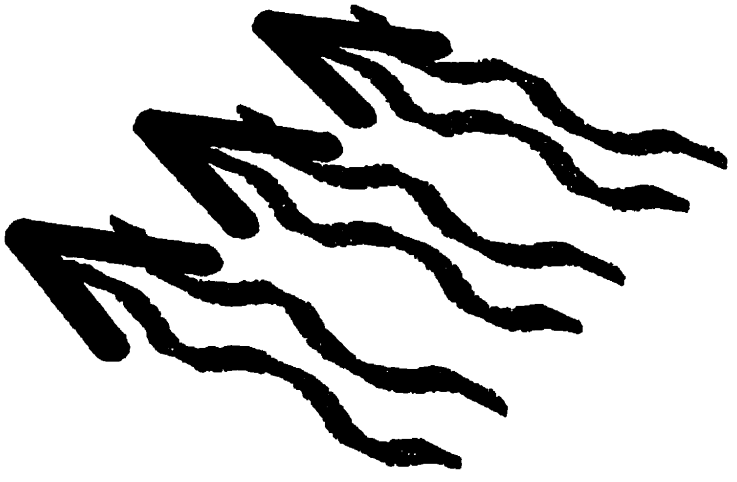

Figure 2.4: Kuethe Vortex Generators

Wheeler (1984, 1991) invented two new types of vortex generator, shown in figures 2.5 and 2.6, based upon the Stephens type. The inventor claims these devices will create more intense vortices than previous designs. If true, the Wheeler-type vortex generators would warrant future investigation.

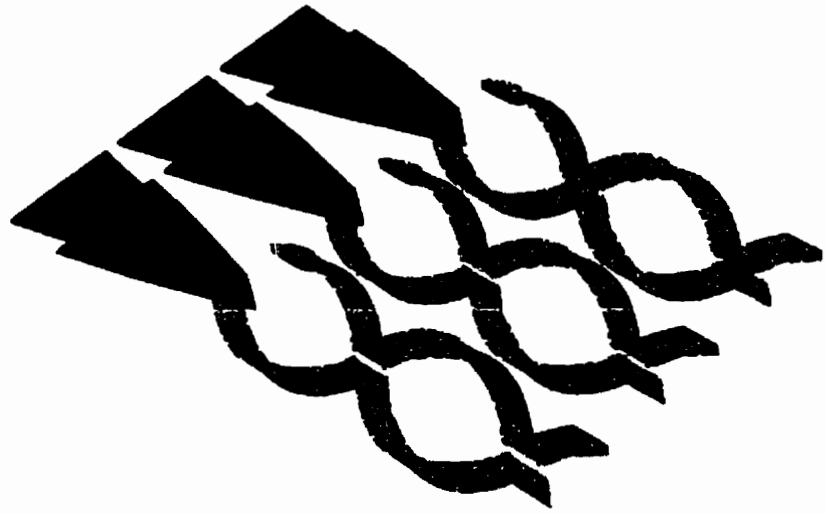

Figure 2.5: Wheeler Type 1 Vortex Generators

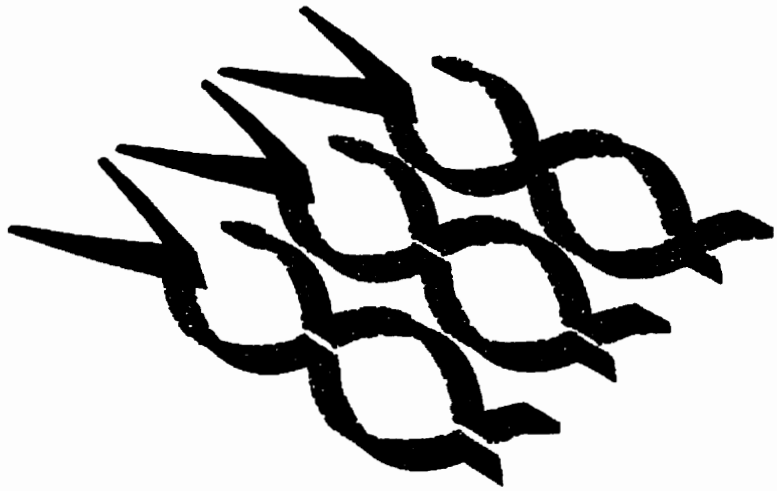

Figure 2.6: Wheeler Type 2 Vortex Generators

2.1.6 Historical Test Methods

2.1.6.1 Static Drag Measurement

The wide variation of human body types combined with the flexibility of limbs and the compliance of soft tissues make repeatable drag measurements with real swimmers extremely

difficult. Nonetheless, various experimenters have attempted 'passive' drag testing of prone swimmers in either flumes or tow tanks. The results of the many researchers are summarized by Clarys (1979). Since most researchers did not measure cross-sectional area, the data could not be normalized. However, Clarys did plot the data together to reveal a range of drag values from 80N to 160N at 2.0m/s.

2.1.6.2 Active Drag Measurement

2.1.6.2.1 Force Deficit/Surplus

Since passive drag measurements are limited to immobile, prone swimmers, attempts have been made to measure the so-called 'active' drag of a moving swimmer. While this quantity is probably impossible to measure directly, various indirect methods have been attempted with, as noted by Clarys (1979), widely varying results.

Several researchers, including Holmér (1974), applied varying known assisting and retarding forces to a swimmer in either a flume or a pool. Oxygen consumption was measured during each phase of the test and for each subject at rest. For a given velocity, the retarding/assisting force was plotted against oxygen consumption. From these values, the researchers extrapolated the theoretical assisting force required to bring the oxygen consumption to the rest level. This assisting force was assumed equal to and opposite the active drag at the given velocity.

Using this approach, it would be difficult to account for changes in propulsive efficiency with varying retarding forces. Competitive swimmers use an 'S' shaped hand pull in order to generate thrust through lift. For an increased load at a given velocity, the swimmer would have to open up the angle of the hand or increase the stroke rate on order to increase thrust. Either of these reactions would result in an effective increase in the hand's angle of attack. Increasing the angle of attack of the hand in order to generate more lift would increase the intensity of the vortex trailing from the fingers. Continuing to increase the load will ultimately cause flow over the hands to stall and the swimmer would be unable to compensate for the load. Consequently, this method probably tends to underestimate the true active drag.

2.1.6.2.2 Force Integration

Hollander et al (1986) and Toussaint et al (1988) conducted tests using transducers with handholds that were placed periodically along a pool lane 0.8 metres below the surface of the water. The swimmers used the handholds to propel themselves. Each transducer recorded the force history on the handhold. By comparing these values with the swimmer's velocity, a value of average active drag was estimated.

2.1.6.2.3 Oxygen Consumption/Heart Rate

This approach to active drag measurement involves taking measurements of an athlete's oxygen consumption while swimming in a pool or flume. From the rate of oxygen consumption, the swimmer's power output can be estimated and compared with their velocity. However, there are a number of error sources with this technique. The human body burns oxygen even when sedentary in order to maintain homeostasis. In addition, during vigorous exercise some portion of the nutrients is burned anaerobically. Consequently, this energy expenditure would not be reflected in the oxygen consumption rate. In any case, the inherent lack of repeatability for all currently known active-drag tests makes them impractical for optimization testing.

3 TEST METHOD AND APPARATUS

3.1 Requirements for Current Test

3.1.1 Realistic Flow Conditions

In designing a test to optimize the vortex generator configuration, a number of requirements arose. Firstly, any chosen test method must produce a flow field in the area of interest that is similar to that for a competitive swimmer. This implies that both the contours of the test article and the Reynolds number must be within the range of real-world experience. These values are shown in section 4.1.1.

3.1.2 Repeatability

Any optimization testing requires repeatable results in order to distinguish between various configurations in a statistically significant manner. This requirement placed constraints on both the measurement apparatus and the test article. The measurement method must give consistently precise readings. The test article must be rigid to avoid geometry variations from one test to the next.

3.1.3 Rapid Turnaround

The need to test a high number of configurations necessitated a test method which would both yield rapid results while allowing quick changeover of vortex configurations.

3.2 Wind Tunnel Testing

3.2.1 Advantages

Considering the above criteria, the closed-circuit low-speed wind tunnel, as described in section 3.4, was chosen for optimization testing. Given a suitable test article, the tunnel was capable of producing Reynolds numbers in the range of competitive swimmers. In addition, the test section was already equipped with a suitably sensitive balance for drag measurement.

3.2.2 Disadvantages

The most obvious disadvantage of wind tunnel testing is the use of air versus water. However, since both air and water are Newtonian fluids, their flow behaviour should be the same at the same Reynolds numbers. Any differences would arise from special cases such as the polymer suit treatments described in section 2.1.4.2. The effects of viscous polymer shedding would be difficult to duplicate in a wind tunnel.

3.3 Test Model

3.3.1 Construction Method

A three-dimensional human computer model was generated and manipulated into the prone position using Poser™ software from Fractal Design Corporation. Three views, as shown in figure 3.1, were printed out in one-half scale. The three views were used to hot-wire a piece of foam-core into the approximate shape. The foam model was then hand shaped and covered with fibreglass.

3.3.2 Specifications

The model dimensions were constrained by the cross-sectional area of the wind tunnel. Rae and Pope (1984) suggest that 5% is the maximum recommended ratio between the model cross-sectional area and that of the wind tunnel. Beyond this, tunnel boundary errors become significant. Given this constraint, a half-scale model of a six-foot male was built with the following dimensions:

- The full length of the model, L, is 1.25m,
- The length from the finger tips to the beginning of the region of interest, L_s, is 0.70m, and
- The cross-sectional area, A, is 0.0194 m^2 which is approximately 5% of the wind tunnel area.

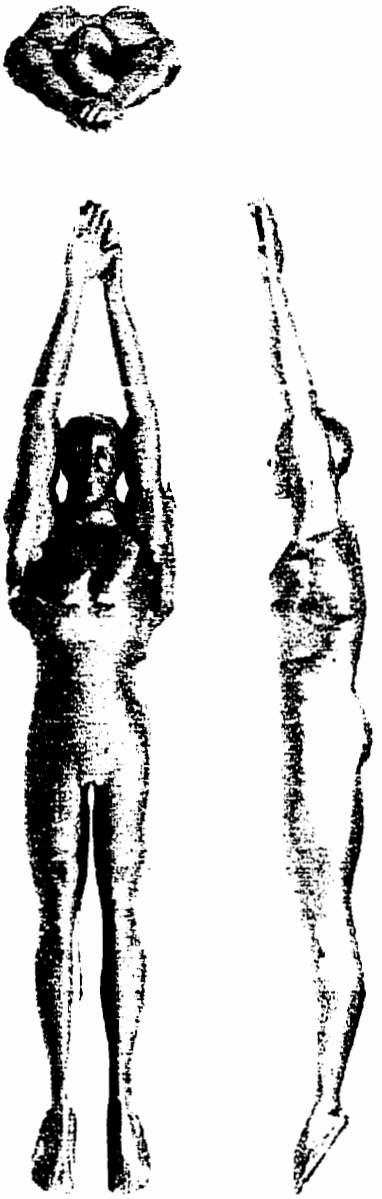

Figure 3.1: Computer Generated Wind Tunnel Model

3.3.3 Model versus Live Swimmer

3.3.3.1 Anthropomorphic Accuracy

Since no two human bodies are the same, any model can at best be said to have a geometry that falls within the space of anatomic possibility. The model contains several simplifications of anatomical detail such as a lack of fingers and toes or distinct facial features. These omissions were due to the limitations of the construction technique that did not lend itself to small detail.

Ultimately, however, the flow patterns in the areas of interest were observed to be similar to those of live swimmers. In addition, the measured drag coefficient was similar to that measured for prone humans at the same Reynolds number.

3.3.3.2 Texture Differences

No attempt was made to model skin texture or hair. The lack of body hair on the model is reasonable considering the near universal practice of shaving all body hair prior to major competitions. In addition, many athletes wear swim caps during competition. Modelling fine-scale skin texture was not possible with the current construction technique.

3.3.3.3 No Skin Compliance

The pliability of human skin may impact boundary layer development. Specifically, a compliant surface will tend to damp out turbulence and may tend to delay boundary layer transition.

3.3.3.4 Repeatability

Even during a single test run, swimmers find it difficult to hold a single body position. Certainly, repeating the same body position precisely from one test to the next is a practical impossibility. Consequently, the use of live swimmers to optimise the vortex generator configuration would be a futile exercise. Given its fixed geometry, the wind tunnel model is clearly superior in this respect.

3.4 Wind Tunnel Description

The closed-circuit low-speed wind tunnel incorporates a removable, closed test section with internal dimensions of 30in x 20in x 72in. The maximum air velocity is approximately 75m/s. However, as discussed in section 4.1.1, testing was limited to approximately 45m/s due to excessive model vibration above that speed.

Wind tunnel velocity is measured via two static pressure taps. One is located in the settling chamber upstream of the test section. The low air velocity in the settling chamber causes this measurement to be close to the stagnation pressure. The second pressure tap is located immediately upstream of the start of the test section. Since the end of the test section is open to

the outside, this measurement is close to atmospheric pressure. The precise relationship between these two pressures and the dynamic pressure in the test section was determined during wind tunnel calibration.

3.5 Force Balance Description

The force balance, shown in figure 3.2, consists primarily of an outer frame from which a platform is suspended by means of linkages. The link arms constrain the motion of the platform to vertical and longitudinal displacement. A pitch arm extends from a pivot that is anchored to the platform. Lift and drag loads result in small displacements of the balance platform. Pitching moments result in angular displacement of the pitch arm. The displacements are measured by linear variable displacement transformers (LVDTs). These transducers contain one primary winding and two secondary. A constant AC voltage is applied to the primary winding. Displacement of the core results in a change in voltage across the two secondary windings. This voltage is recorded using a digital multi-meter or other data acquisition device. The voltages are converted to forces or moments using constants determined during balance calibration.

The model was suspended in the test section from two bayonets and a pitch strut as shown in figure 3.3. The bayonets and pitch strut transmit lift, drag and pitch loads to the force balance. Only the balance platform is shown for clarity.

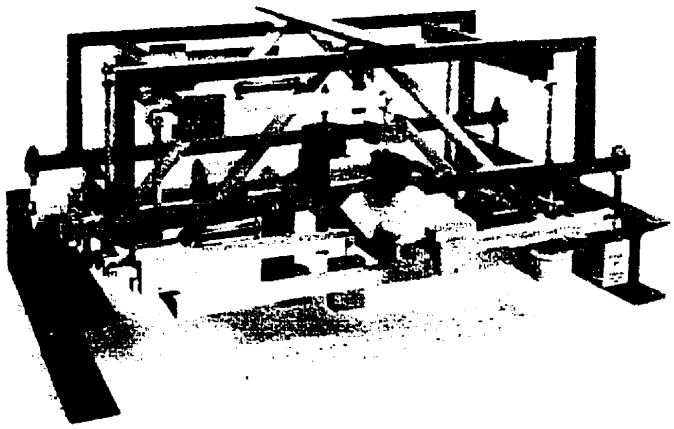

Figure 3.2: Wind Tunnel Balance

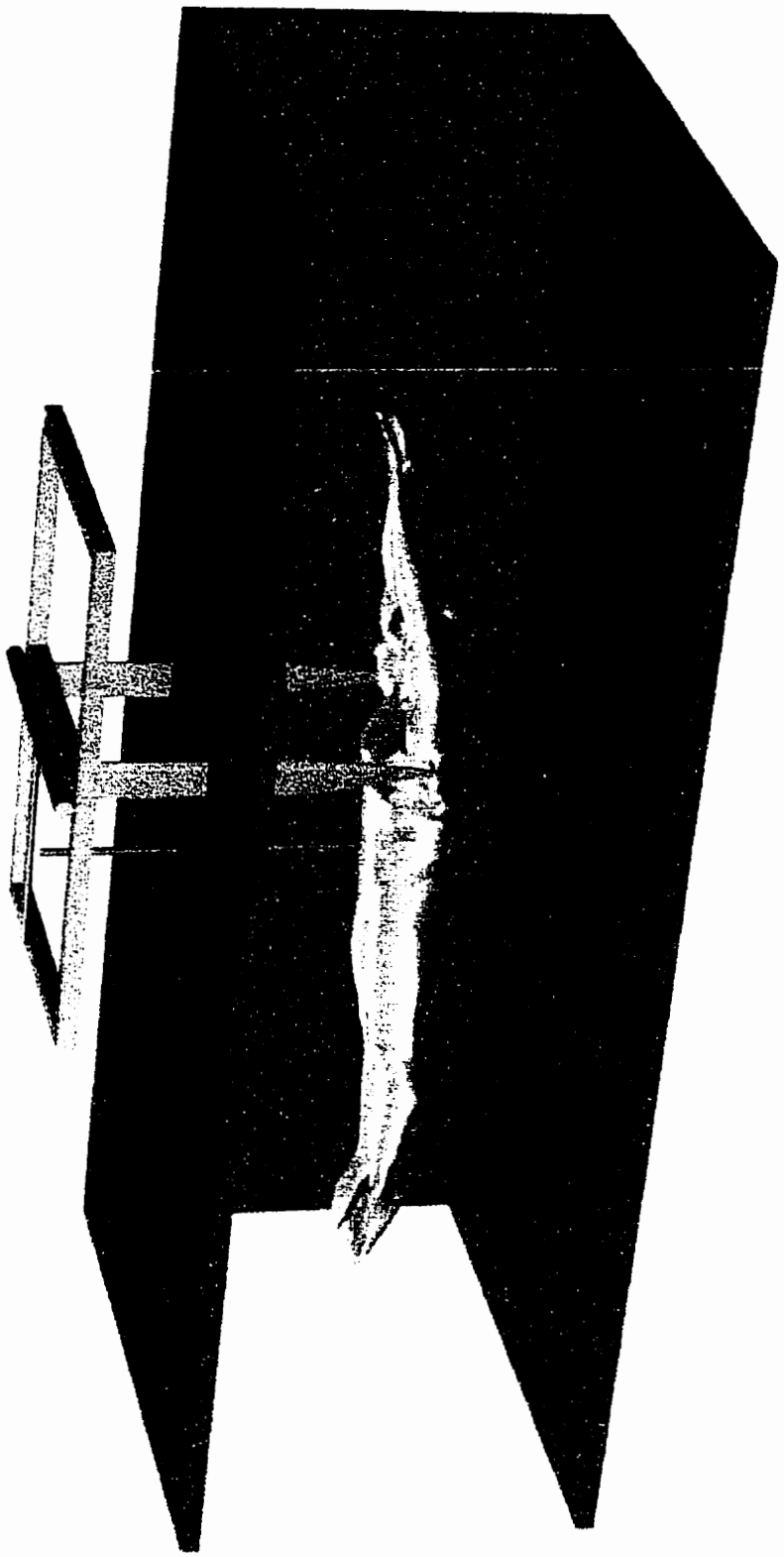

Figure 3.3: Model Suspended in Test Section

4 RESULTS AND DISCUSSION

4.1 Operating points

4.1.1 Reynolds Number

The model was tested without vortex generators attached in order to debug the apparatus, and determine baseline drag values against which to compare modified configurations. The initial baseline testing revealed several minor problems with the apparatus. For instance, the holes for the main struts had to be enlarged slightly to prevent rubbing at higher wind tunnel speeds.

A more serious problem developed when it was discovered that the model tended to vibrate above 60% wind tunnel speed or about 45m/s. In order to assess the applicability of testing in this lower velocity range, the Reynolds numbers for the model and elite swimmers were compared. The Reynolds number for the model at the maximum tested velocity is determined as follows:

Given that

$L = 1.25m$,

where L is the full length of the model,

$V = 45\,m/s$,

$\rho_{Air} = 1.19\,kg/m^2$, and

$\mu_{Air} = 18.3 \times 10^{-6}\,kg/m\,s$,

the Reynolds number for the model is

$$\mathrm{Re} = \frac{\rho LV}{\mu} = \frac{(1.19)(1.25)(45)}{18.3 \times 10^{-6}} = 3.7 \times 10^{6}.$$

A petite female 200m breaststroker (the shortest swimmer in the slowest race) would produce the lowest Reynolds number amongst world class swimmers. The Reynolds number during the glide phase after a start or turn with arms extended overhead is determined as follows:

Given that

$L \approx 2.0m$,

where L is the full length of the swimmer with arms extended overhead and toes pointed,

$$V = \frac{200m}{146s} = 1.37\,m/s,$$

$\rho_{H_2O} = 996\,kg/m^2$, and

$\mu_{H_2O} = 905 \times 10^{-6}\,kg/m\,s$,

the Reynolds number for the small female breaststroker is

$$\mathrm{Re} = \frac{\rho LV}{\mu} = \frac{(996)(2.0)(1.37)}{905 \times 10^{-6}} = 3.0 \times 10^6.$$

Similarly, a male 50m freestyler (the tallest swimmer in the fastest race) generates the upper limit of Reynolds number. His length and velocity are

$L \approx 2.5m$, and

$$V = \frac{50m}{21.9s} = 2.28\,m/s.$$

Thus, the Reynolds number for the male sprint freestyler is

$$\mathrm{Re} = \frac{\rho LV}{\mu} = \frac{(996)(2.5)(2.28)}{905 \times 10^{-6}} = 6.3 \times 10^6.$$

Consequently, the uppermost Reynolds numbers of the tests were within the range of interest.

4.1.2 Angle of Attack

The angle of attack for a live swimmer is variable due to the body's flexibility and changes in body dimensions from one athlete to the next. The most desirable body position is one that minimizes drag. This, however, is complicated by buoyancy effects. Maintaining a given depth during the submerged glide phase requires the swimmer to modify the angle of attack in order to create lift that cancels the buoyancy force. Since the body is not symmetrical front to back, the required angle of attack relative to the swimmer will vary with body rotation. Depending on the stroke and individual style, the swimmer may be swimming on their back, front, or side when submerged.

A test was conducted to establish the variability of drag coefficient with angle of attack. The results of the test are shown in figure 4.1. With the wind tunnel speed set at 30.4 m/s, the angle of attack of the model was varied by adjusting the pitch angle (an adjustment external to the test section) on the balance with the wind tunnel running. Maintaining a constant velocity eliminated any change in drag coefficient that might arise due to Reynolds number variability. The pitch angle shown on the graph is not the true angle of attack. It is simply the pitch angle reading on the balance.

The pitch angle for all subsequently reported testing is -5°. The measured drag coefficient at this pitch angle was 0.537. This is only slightly higher than the minimum value of 0.535 measured at -7°. However, since there was a sharp increase in drag coefficient to 0.624 at -8°, a test pitch angle of -7° could be prone to repeatability errors. Conversely, the observed drag coefficient for -3° was 0.548. Consequently, a pitch angle of -5° provides a drag coefficient which is within 0.4% of the minimum while showing a maximum variability of 2.0% for changes in angle of attack as great as 2°.

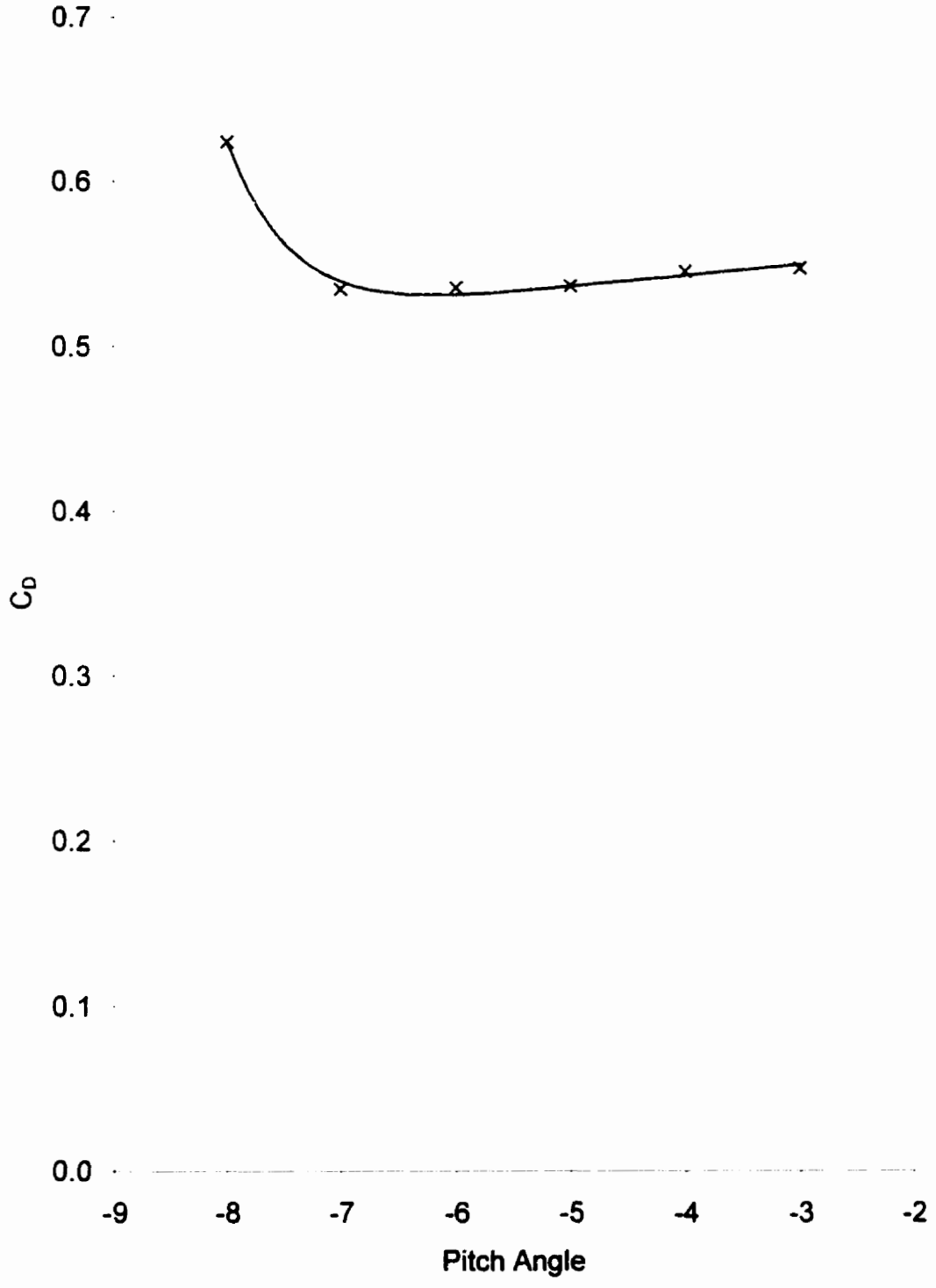

Figure 4.1: Variation of Drag Coefficient with Pitch Angle

4.2 Measurement Accuracy and Repeatability

The accuracy of the measured drag coefficient will be affected by the uncertainty in the following variables:

- The Drag Transducer Output. Based on the balance acceptance calibration, the linear variable displacement transformer (LVDT) used to measure the drag force showed a constant bias error of 0.04N across the range measured in our experiment, about 6N to 15N. Consequently, the bias error in the calculated coefficient of drag would range from 0.3% to 0.7%.

- The Model Cross-sectional Area. The model cross-sectional area was estimated by external measurements to be $0.0194m^2$. This value is probably accurate to $\pm 0.001m^2$. This would contribute an error in the coefficient of drag estimate of 5%. However, since this is a systematic error, it will have no effect on the ranking of results.

- The Tare Drag Estimate. The drag on the struts and bosses holding the model would normally be measured directly without the model installed. This drag is then subtracted from all measurements with the model installed. These measurements were scheduled for after completion of model testing. Unfortunately, the balance experienced a mechanical failure that could not be fixed prior to the wind tunnel being taken over for other experiments. However, a reasonable estimate of the tare drag could be made based on the geometry of the fixtures. While the accuracy of this estimate is probably only within ±15%, this would have no effect on the ranking of the various configurations. Furthermore, since the tare drag constitutes about 24% of the measured drag, the absolute accuracy of the drag coefficient would only be decreased by about 4%.

- Pitch Angle. As discussed in section 4.1.2, the maximum variation in drag coefficient of 2.0% was measured for variations in pitch angle of up to 2°. Random error could result from variability in model reinstallation. The pitch angle adjustment scale is accurate to 1°. Using this value the maximum random error resulting from errors in installation from one run to the next would be 1.2%. The bias error for pitch angle is not relevant since, as discussed in section the pitch angle was chosen arbitrarily.

- Dynamic Pressure. The stagnation pressure in the test section was calculated from static pressure measurements of the wind tunnels settling chamber, *Pc1*, and a pressure tap immediately upstream of the test section, *Pc2*. In order to estimate the random error in the dynamic pressure q, one notes that based on wind-tunnel calibration,

$$P_0 = \frac{P_{c1} - P_{c2}}{0.938} + P_\infty \tag{4.1}$$

and

$$q = P_0 - P_\infty, \tag{4.2}$$

where P_∞ is the static pressure in the test section and is assumed to be equal to P_{atm}, the outside air pressure, since the end of the test section is vented to the room.

Combining 4.1 and 4.2 gives

$$q = \frac{P_{c1} - P_{c2}}{0.938}. \tag{4.2a}$$

P_{c1} and P_{c2} were measured using a manometer that could be read to an accuracy of ±0.01in H_20 or ±2.5Pa while the measured dynamic pressure varied from approximately 530 to 1240Pa. The coefficient of drag is calculated from the equation

$$C_D = \frac{D}{A \cdot q}, \tag{4.3}$$

where D is the drag force and A is the model cross-sectional area. Substituting equations 4.1 and 4.2 into 4.3 gives

$$C_D = \frac{D \cdot 0.938}{A(P_{c1} - P_{c2})}. \tag{4.4}$$

Including the random error of 2.5Pa that applies to both P_{c1} and P_{c2}, this can be rewritten as

$$C_D = \frac{D \cdot 0.938}{A(P_{c1} - P_{c2} \pm 5)}. \tag{4.5}$$

The random percentage error in the calculated drag coefficient resulting from errors in pressure measurement is given by the expression

$$\%ERR = \frac{C_{Dmeas} - C_{Dtrue}}{C_{Dtrue}} \cdot 100\%. \tag{4.6}$$

Substituting in equations 4.4 and 4.5 gives

$$\%ERR = \frac{(P_{c1} - P_{c2} + 5)^{-1} - (P_{c1} - P_{c2})^{-1}}{(P_{c1} - P_{c2})^{-1}} \cdot 100\%. \tag{4.7}$$

Rearranging equation 4.2a gives

$$P_{c1} - P_{c2} = q \cdot 0.938. \tag{4.8}$$

For the minimum tested dynamic pressures of 540Pa we have

$$P_{c1} - P_{c2} = (540)(0.938) = 507Pa.$$

Substituting this into equation 4.7 gives

$$\%ERR = \frac{(507 + 5)^{-1} - (507)^{-1}}{(507)^{-1}} \cdot 100\% = 1.0\%.$$

Similarly, for the maximum tested dynamic pressure of 1240Pa we have

$$P_{c1} - P_{c2} = (1240)(0.938) = 1163Pa.$$

Again substituting into 4.7 gives

$$\%ERR = \frac{(1240 + 5)^{-1} - (1240)^{-1}}{(1240)^{-1}} \cdot 100\% = 0.4\%.$$

Consequently, the random error in drag coefficient arising from pressure measurement errors can be expected to range from 0.4% to 1.0%. Dynamic pressure is calculated from the difference of the two pressure measurements. Since both manometers connect to the same reservoir, any bias errors would tend to cancel out.

- Temperature. The static temperature gauge is graduated at intervals of 2°F. In addition, the temperature probe was placed upstream of the test section in a lower velocity flow. Consequently, the measured temperature is somewhere between the static temperature and the total temperature. The ratio of static to total temperature is given by Barlow et al (1999) as:

$$\frac{T_{tot}}{T} = \left[1 + \left(\frac{\gamma - 1}{2}\right) M^2\right], \tag{4.9}$$

where γ is the ratio of specific heats and M is the Mach number. For air at 75°F, a typical measured test temperature,

$\gamma = 1.402$.

The Mach number is given by

$$M = \frac{V}{a}, \tag{4.10}$$

where a is the speed of sound and is given by

$$a = \sqrt{\gamma RT}\,. \tag{4.11}$$

For air this becomes

$a = 20.04\sqrt{T}$ m/s.

At 75°F this is

$a = 20.04\sqrt{297K} = 345$ m/s.

Across the test velocity range of 30m/s to 47m/s the Mach number varies between

$$M_1 = \frac{30\,m\ s}{345\,m\ s} = 0.087$$

and

$$M_2 = \frac{47\,m\ s}{345\,m\ s} = 0.136.$$

The ratio of static to total temperature for the high and low speeds is

$$\frac{T_{tot1}}{T_1} = 1 + \left(\frac{1.402 - 1}{2}\right)(0.087)^2 = 1.0015$$

and

$$\frac{T_{tot2}}{T_2} = 1 + \left(\frac{1.402 - 1}{2}\right)(0.136)^2 = 1.0037.$$

At 30m/s and a static temperature of 75°F or 535°R the error is

$$T_{tot1} - T_1 = T_1 \cdot \frac{T_{tot1}}{T_1} - T_1 = (535)(1.0015) - 535 = 0.8\,°\text{F}.$$

Similarly, at 47m/s the error is

$$T_{tot2} - T_2 = T_2 \cdot \frac{T_{tot2}}{T_2} - T_2 = (535)(1.0037) - 535 = 2.0\,°\text{F}.$$

Consequently, the error in static temperature measurement due to sensor shape and position should not exceed 2.0°F. Whatever the true value it will be a bias error and thus systematic.

In order to assess the impact of the anticipated temperature errors on Reynolds number and ultimately drag coefficient, we note that velocity is derived from the measured dynamic pressure using the equation

$$V = \sqrt{\frac{2q}{\rho}}. \tag{4.12}$$

Substituting this into the Reynolds number formula gives

$$\mathrm{Re} = \frac{\rho L\sqrt{\frac{2q}{\rho}}}{\mu} = \frac{L\sqrt{2q\rho}}{\mu}. \tag{4.13}$$

Using this formula, assuming a temperature of 75°F and a dynamic pressure of 540Pa (approximately the lowest tested), the Reynolds number for the model is given by

$$\mathrm{Re}_{75F,540Pa} = \frac{1.25\sqrt{2(540)(1.188)}}{1.833\times10^{-5}} = 2.442\times10^{6}$$

Similarly for 73°F and 77°F we have

$$\mathrm{Re}_{73F,540Pa} = \frac{1.25\sqrt{2(540)(1.192)}}{1.828\times10^{-5}} = 2.454\times10^{6}$$

$$\mathrm{Re}_{77F,540Pa} = \frac{1.25\sqrt{2(540)(1.183)}}{1.838\times10^{-5}} = 2.431\times10^{6}$$

Likewise at 1280Pa (approximately the highest tested pressure), the Reynolds numbers for 73°F, 75°F and 77°F are:

$$\mathrm{Re}_{73F,1280Pa} = \frac{1.25\sqrt{2(1280)(1.192)}}{1.828\times10^{-5}} = 3.778\times10^{6}$$

$$\mathrm{Re}_{75F,1280Pa} = \frac{1.25\sqrt{2(1280)(1.188)}}{1.833\times10^{-5}} = 3.760\times10^{6}$$

$$\mathrm{Re}_{77F,1280Pa} = \frac{1.25\sqrt{2(1280)(1.183)}}{1.838\times10^{-5}} = 3.743\times10^{6}$$

The impact of this variation on drag coefficient can be estimated by noting its relationship with Reynolds number as observed during baseline testing. Of the two baseline tests, as described in section 4.5, the clean baseline showed the greatest dependence on Reynolds number. As will be derived in section 4.6.1, the data curve fit for the clean baseline is given by

$C_D = -0.0611 Log\ Re + 0.9151.$

Using this relation for a dynamic pressure of 540Pa, the calculated drag coefficients for 73°F, 75°F and 77°F are

$C_{D73F,540Pa} = 0.52449$

$C_{D75F,540Pa} = 0.52462$, and

$C_{D77F,540Pa} = 0.52474.$

Similarly for a dynamic pressure of 1280Pa the drag coefficients are

$C_{D73F,1280Pa} = 0.51304$

$C_{D75F,1280Pa} = 0.51316$, and

$C_{D77F,1280Pa} = 0.51329.$

The percentage error associated with these deviations is given by

$$\%ERR = \frac{C_{D2} - C_{D1}}{C_{D1}} \cdot 100\% \qquad (4.14)$$

Using this equation, the percentage errors in C_D due to a 2°F error in temperature are

$\%ERR_{540Pa} = \pm 0.024\%$

$\%ERR_{1280Pa} = \pm 0.026\%$

Both the random error due to instrumentation limitations and the maximum bias error due to measuring a temperature that is not static are 2°F. Consequently, one can expect that neither the bias error nor the random error in drag coefficient due to temperature measurement error should exceed approximately 0.025%. Since this is significantly less than the 0.4% to 1.0% error associated with pressure measurement, no attempt was made to correct the temperature to true static.

4.3 Wind Tunnel Boundary Errors

- Horizontal Buoyancy. Boundary layer growth along the walls of the tunnel will cause a variation in cross-sectional area along the test section. This in turn will cause a static pressure variation along the tunnel. In the case of the test section used in this experiment which has flat, parallel sides, the static pressure will decrease along the tunnel. This will result in an increase in drag on the model over that which it would experience in an unbounded flow.

- Solid Blockage. The finite ratio of model cross-sectional area to tunnel flow area results in an increase in surface stresses over what the model would experience in an unbounded flow.

- Wake Blockage. The finite ratio of the wake area and the tunnel area results in an increase in drag on the model over what it would experience in an unbounded flow.

- Solid and Wake Blockage Error Estimate. Barlow et al (1999) give the following approximate formula for the combined error in measured drag due to solid and wake blockage:

$$\%ERR = \frac{1}{4} \cdot \frac{\text{model frontal area}}{\text{test - section area}} \cdot 100\%$$

In this case, the model frontal area includes that of the mounting hardware. Inserting the appropriate values for this test gives:

$$\%ERR = \frac{1}{4} \cdot \frac{0.0194 + 0.0036}{0.3871} \cdot 100\% = 1.5\%$$

- Significance of Tunnel Boundary Errors. All of the tunnel boundary errors are systematic. Since these experiments are primarily concerned with relative changes in drag, it would not be relevant to apply the tunnel boundary corrections. In addition, the model represents only one possible body geometry. The variability in measured drag coefficients for live swimmers as discussed in section 2.1.1 would overwhelm any tunnel boundary correction applied to this test model.

4.4 Summary of Bias and Random Errors

The following table summarizes the assumed bias and random errors in drag coefficient arising from the various sources discussed in sections 4.2 and 4.3:

ERROR SOURCE	*RANDOM %ERROR*	*BIAS %ERROR*
Drag Transducer (LVDT)	~ 0	0.3 to 0.7
Model Cross-sectional Area	0	<5
Tare Drag Estimate	0	<4
Pitch Angle	<1.2	N/A
Dynamic Pressure	<1.0	~ 0
Static Temperature	<0.03	<0.03
Tunnel Boundary Errors	~ 0	~ 1.5

The bias errors are systematic and will affect neither the ranking of results nor the estimated percentage difference in drag from one configuration to the next. In addition, the wide variation in geometry and therefore drag coefficient amongst swimmers (0.58 to 1.04 as discussed in section 2.1.1) makes bias error corrections on the order of 5 to 10% somewhat irrelevant.

The clean baseline test as described in section 4.5 was the most extensively tested configuration with 31 data points. The variability in the measured drag coefficient about the regression line was approximately ±1.5%. This is within the predicted range of random error associated with the two dominant sources of random error, pitch angle and dynamic pressure.

4.5 Test Results for Baseline Configurations

Two types of baseline test were conducted. The Stephens type vortex generators were initially mounted on a fabric strip that was then affixed to the model. This strip of flexible swimsuit material was employed in order to facilitate attachment to the contours of the model and to maintain the relative positions of the vortex generators from one test to the next. The fabric used had a thickness of ~0.01in as did the double sided tape used to affix the material to the model. In order to assess the affect of the vortex generators alone on drag, baseline testing was conducted with a fabric strip affixed to the posterior of the model. The fabric strip used in baseline testing was 0.6in wide and 7in long. The strip was affixed to the model such that its forward edge was 1.0in forward of the apex of the posterior. This was a typical size and location of the fabric strips later used to attach the vortex generators to the model.

Initially, it was assumed that while the fabric strips would influence drag, they would not have a significant interaction with the vortex generators. That is to say, the drag influence of the fabric strips and the vortex generators would be simply additive. As will be discussed in section 4.8.8, this assumption proved to be untrue.

Figure 4.2 shows the variation of the drag coefficient with Reynolds number for the two baseline configurations. Regression curves were fit to the data using the least squares method. Using the method described in Lipson and Sheth (1973), confidence bands were fit to the data. The outer confidence band is the region into which 90% of all measurements should fall. The inner band is the region in which one can be 90% certain of finding the true mean of the data. The method used is described in more detail in section 4.6.1.

The range of Reynolds numbers is shown from 2.0×10^6 to 7.0×10^6. This gives an idea of the extrapolated values of the drag coefficient across the entire region of interest. The expanded confidence interval farther into the extrapolated region of the graphs reflects the increased uncertainty in the coefficient of drag as the Reynolds number increases above the actually tested values.

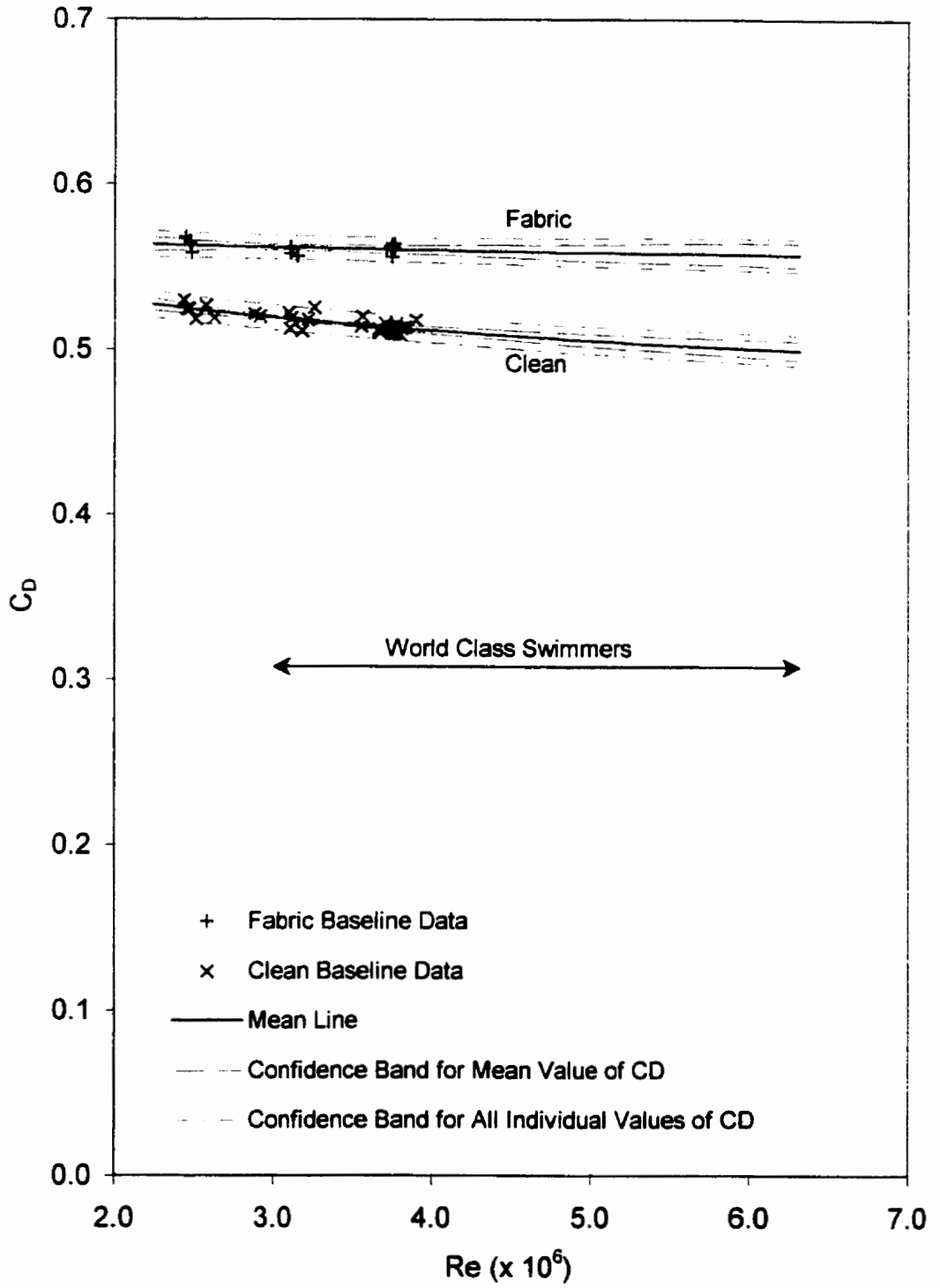

Figure 4.2: Drag Coefficient versus Reynolds Number for Baseline Configurations

4.6 Discussion of Results for Baseline Configurations

4.6.1 Baseline Data Repeatability

The true relationship of drag versus velocity was assumed to take the form:

$$C_D = a\ Log\ Re + b \tag{4.15}$$

The constants a and b were determined for the two baseline configurations using the function LINEST() found in Microsoft Excel. Using this function, the regression equation for the fabric baseline was found to be

C_D = -0.0138**Log Re* + 0.6508.

Similarly the regression equation for the clean baseline was

C_D = -0.0611**Log Re* +0.9151.

These lines represent the mean for the measured data. The sample size is, however, limited. In order to assess the probability that these equations describe the true relationship between Reynolds number and drag coefficient (plus or minus any bias errors), one must calculate the confidence bands around the data. The inner confidence band contains the true mean to the specified confidence level and is defined as

$$A_1 = \pm t_{\alpha/2;(n-2)} S_{y \bullet x} \sqrt{\frac{1}{n} + \frac{(1-\bar{x})^2}{(n-1)S_x^2}}, \tag{4.16}$$

where $t_{\alpha/2;(n-2)}$ is the value of the Student's t-distribution for $1 - \alpha$ = the confidence level,

$$S_x = \sqrt{\frac{\sum_{i=1}^{n}(x_i - \bar{x})^2}{n-1}}, \text{ and} \tag{4.17}$$

$$S_{y \bullet x} = \sqrt{\frac{\sum_{i=1}^{n}(y_i - y_{ic})^2}{n-2}}. \tag{4.18}$$

These are the standard forms of the equations. For this study $y = C_D$ and $x = Log\ Re$.

The outer band contains all data points to the desired confidence level and is given by

$$A_2 = \pm t_{\alpha/2;(n-2)} S_{y \bullet x} \sqrt{1 + \frac{1}{n} + \frac{(1-\bar{x})^2}{(n-1)S_x^2}}. \qquad (4.19)$$

The average values of the outer confidence band, A_2, for the clean and fabric baselines was 1.5% and 1.3% respectively. These values compare well with the estimated maximum random errors of 1.0% and 1.2% produced by dynamic pressure and pitch angle.

4.6.2 Comparison with Historical Results

The estimated drag coefficient for the fabric baseline ranged from approximately 0.56 to 0.57. This is very close to the lower limit of 0.58 from previous studies on live swimmers (Clarys, 1978b). This should be expected since previous studies include swimmers of varying skill levels. One would anticipate that elite competitive swimmers would tend towards the lower end of the range. They train extensively to hold the optimal 'streamlined' position. The body position of the model is based on this position which experience indicates is the most efficient. Consequently, the drag coefficient, at least, does not indicate a gross discrepancy in flow characteristics from the model to a live swimmer.

4.6.3 Differences between Two Baseline Results

The presence of the fabric strips increased the measured drag coefficient for the model by an average of approximately 8%. In addition, the coefficient of drag for the fabric baseline showed a decreased variability with Reynolds number in comparison with the clean baseline. This result is similar to the effect of surface roughening on a cylinder as shown in White (1991). Between Reynolds numbers of approximately 5×10^4 and 5×10^5, surface roughness causes a decrease in overall drag due to separation delay. However, at Reynolds numbers above 5×10^5, surface roughness has an adverse impact on overall drag. In order to determine the precise cause, a more detailed study of the boundary layer conditions upstream of the posterior separation bubble is required.

4.7 Vortex Generator Testing

4.7.1 Choosing a Vortex Generator Height Based on Boundary Layer Estimates

In order to make a reasonable estimate for the initial height of the vortex generators, one must estimate the boundary layer conditions in the area of interest. Since the geometry of the vortex generators was ultimately to be determined by experiment, a simple flat-plate estimate was performed. From the model geometry discussed earlier, the tested Reynolds number immediately upstream of the posterior separation bubble, Re_s, ranges from

$$Re_s = \frac{\rho L_s V}{\mu} = \frac{(1.19)(0.70)(30)}{18.3 \times 10^{-6}} = 1.4 \times 10^6$$

to

$$Re_s = \frac{\rho L_s V}{\mu} = \frac{(1.19)(0.70)(45)}{18.3 \times 10^{-6}} = 2.0 \times 10^6,$$

where L_s is the distance from the leading edge of the model to the apex of the posterior.

Similarly, for world-class swimmers, the Reynolds number immediately upstream of the posterior separation bubble ranges from

$$Re_s = \frac{\rho L_s V}{\mu} = \frac{(996)(1.12)(1.37)}{905 \times 10^{-6}} = 1.69 \times 10^6$$

for a female 200 metre breaststroker, to

$$Re_s = \frac{\rho L_s V}{\mu} = \frac{(996)(1.4)(2.28)}{905 \times 10^{-6}} = 3.5 \times 10^6$$

for a male 50m freestyler.

All of these Reynolds numbers lie within the possible transition range for flat plates of $5 \times 10^5 < Re_s < 8 \times 10^7$ (White, 1979). Since a swimmer is clearly not a flat, smooth plate, one

would expect transition to occur toward the lower end of the range. This may, however, be somewhat mitigated by the compliance of the swimmers skin that would tend to damp out turbulence and delay separation. In order to examine the possible range of conditions for the boundary layer, its thickness was calculated for both laminar and turbulent assumptions. The thickness of a laminar boundary layer on a flat plate is given by Kuethe and Chow (1986) as

$$\delta = \frac{5.2x}{\sqrt{\mathrm{Re}_x}}. \tag{4.20}$$

For the female breaststroker this gives

$$\delta = \frac{(5.2)(1.12)}{\sqrt{1.69\times10^6}} = 4.48mm,$$

and for the male freestyler,

$$\delta = \frac{(5.2)(1.4)}{\sqrt{3.5\times10^6}} = 3.89mm.$$

The narrow range of these values suggest that, at least for the laminar assumption, a single vortex generator height might be adequate for all world class swimmers. Now, assuming the boundary layer to be fully turbulent from the leading edge, its thickness is given by Kuethe and Chow as

$$\delta = \frac{0.37x}{\mathrm{Re}_x^{1/5}}. \tag{4.21}$$

For the female breaststroker this gives

$$\delta = \frac{(0.37)(1.12)}{(1.69\times10^6)^{1/5}} = 23.5mm$$

and for the male freestyler,

$$\delta = \frac{(0.37)(1.4)}{(3.5\times10^6)^{1/5}} = 25.4mm$$

The estimated turbulent boundary layer thickness also varies little across the range. This reinforces the suggestion that a single vortex generator height would be equally effective for all elite swimmers. That being said, the vast difference between the laminar and turbulent boundary layer heights might seem to impose a wide range on possible vortex generator heights. However, a closer examination of the velocity profiles for laminar and turbulent layers suggests that a single vortex generator height will be satisfactory for both possibilities.

In the case of the turbulent layer, most of the velocity change occurs close to the wall. This suggests that even a vortex generator that is very short in comparison with the boundary layer thickness will be effective in increasing shear stress at the wall thereby delaying separation. Indeed Lin et al (1990) found that even vortex generators as short as 0.1δ were effective in controlling turbulent boundary layer separation.

Conversely, the more gradually sloped laminar boundary layer would require, relative to its height, a much larger vortex generator. Laminar flow separation is generally delayed by simply tripping the boundary layer into turbulence by means of either surface roughness or a transverse obstacle. However, this produces a natural turbulent boundary layer (NTL) which has less eddy viscosity and is therefore less effective at separation control than the artificial turbulent boundary layer (ATL) produced by vortex generators (Kuethe, 1972).

A first guess at an appropriate vortex generator height was chosen as 0.25 of the estimated turbulent boundary layer thickness. This would translate into a height of 6mm on a swimmer. For the model, the assumed turbulent boundary layer thickness is estimated for the highest test speed to be

$$\delta = \frac{(0.37)(0.7)}{(2.0\times10^{6})^{1/5}} = 14.2mm$$

This is approximately half the predicted turbulent boundary layer thickness for the world class swimmers. Consequently, a height of 3mm was chosen for the initial tests of the Stephens vortex generators.

4.8 Vortex Generator Configuration Screening

4.8.1 Vortex Generator Design Variables

In order to find a viable configuration, one must first identify the important variables for vortex generator design. In order to reduce the degrees of freedom, most of the variables were fixed based on either analysis or recommendations of previous researchers. The variables were either fixed or constrained as follows:

- Type. The Stephens type was initially chosen due to its ease of manufacture and the variety of available research. Due to end-user concerns, the Kuethe type was later adopted for its lower profile and lack of sharp protrusions.

- Angle of Attack. This is applicable to the Kuethe type. The smaller type 1 Kuethe vortex generators that were tested initially were constrained by the Dymo-Labeller as discussed in section 4.9.1. It could produce only a single angle of approximately 22.5°. The larger type 2 Kuethe used an angle of 15° as suggested by Kuethe and Chow (1986).

- Ramp Angle. This is applicable to the Stephens Type. A ramp angle of 10° was chosen in order to produce as compact a design as possible without adversely affecting efficiency. The efficiencies for various NACA duct ramp angles are given in the Royal Aeronautical Society data sheet RAS 66029 (1981).

- Height. The Stephens vortex generator height was fixed at 3mm on the model based on the analysis performed in section 4.7.1.

- Number of Rows. The number of rows was limited to a maximum of three in order to minimize weight and potential manufacturing cost.

- Number of Vortex Generators within Each Row. This variable was limited first by the number of vortex generators required to span the width of the separation bubble. A secondary restraint was imposed by the width of material on a swimsuit.

- Longitudinal Position of Vortex Generators. Lin et al (1990) suggested that vortex generators should be placed approximately 2δ upstream of baseline separation initiation. The estimate

of turbulent boundary layer thickness performed in section 4.7.1 gave a boundary layer thickness of 14.1mm on the model. Consequently, the value of 2δ is 28.2mm or about 1.1in. Given this, the first row of vortex generators was placed 1.25in, 1.0in or 0.75in ahead of the apex of the posterior. Based on observations of tufts placed in the region of interest during baseline testing, the apex was observed to be the approximate initiation line of separation.

- Lateral Spacing between Vortex Generators. For the Stephens vortex generators the spacing was fixed to that dictated by the NACA duct geometry as described in RAS 66029 (1981). The spacing of the type 1 Kuethe vortex generators was dictated by the spacing produced by the Dymo-Labeller. The spacing of the type 2 Kuethe vortex generators was equal to their width as suggested by Rao and Kariya (1988).

- Spacing between Rows. The spacing between rows of Stephens vortex generators was set to zero. This was done in order to approach the proprietary Wheeler design of overlapping Stephens vortex generators as shown in figure 2.5. Lin et al (1990) found this an effective arrangement for separation control.

- Relative Lateral Alignment of Vortex Generators from one Row to the Next. In all tests, the vortex generators in succeeding rows were aligned directly behind those in the first row. This was done in order to reinforce the vortices created in the first row rather than create new potentially interfering vortices.

4.8.2 Minimum Required Drag Reduction

Obviously, any viable configuration must reduce drag by some significant amount. In order to define 'significant', one must examine the relationship between drag and the elapsed time for a race, the quantity of interest to the end user. The following is a simplified analysis intended to identify the approximate relationship between elapsed time and drag coefficient. The relationship between velocity, power, and drag is given by:

$$P' = DV . \tag{4.22}$$

where P' is the usable power, D is the drag, and V is the velocity. The usable power is given by

$$P' = \eta P , \tag{4.22a}$$

where η is the overall propulsive efficiency and P is the power generated by the swimmer.

Noting that drag is related to velocity by

$$D = C_D A \frac{1}{2} \rho V^2, \tag{4.23}$$

where C_D is the drag coefficient, A is the cross-sectional area of the swimmer, and ρ is the water density, and substituting equations 4.23 and 4.22a into 4.22 gives

$$\eta P = C_D A \frac{1}{2} \rho V^3. \tag{4.24}$$

As one would expect, maximum human power decreases with increasing duration as shown in Figure 4.3 (Abbott and Wilson, 1995). Near sixty seconds, a typical duration for a 100-metre race, the maximum power output is approximated by

$$P = 1130 - 9.73t \tag{4.25}$$

where t is the duration of the race in seconds. The average velocity during the race is given by

$$V = \frac{S}{t}, \tag{4.26}$$

where S is the race distance. Substituting equations 4.25 and 4.26 into 4.24 gives

$$\eta(1130 - 9.73t) = C_D A \frac{1}{2} \rho \frac{S^3}{t^3}. \tag{4.27}$$

Since we are interested in the relationship between C_D and t, equation 4.27 can be rearranged as

$$\eta 1130t^3 - \eta 9.73t^4 = C_D A \frac{1}{2} \rho S^3, \tag{4.27a}$$

which becomes

$$C_D = \frac{2\eta(1130t^3 - 9.73t^4)}{A\rho S^3}. \tag{4.27b}$$

The above equation is only valid for races that are close to 60 seconds in duration. Assuming we wish to reduce the elapsed time for a 100-metre race from 60 seconds to 59.5 seconds, the required drag reduction would be given by

$$\frac{C_{D59.5}}{C_{D60.0}} = \frac{(1130)(59.5)^3 - (9.73)(59.5)^4}{(1130)(60)^3 - (9.73)(60)^4} = 0.979.$$

Similarly, for a 0.1-second reduction in elapsed time, the relative required drag coefficient is given by

$$\frac{C_{D59.9}}{C_{D60.0}} = \frac{(1130)(59.9)^3 - (9.73)(59.9)^4}{(1130)(60)^3 - (9.73)(60)^4} = 0.996.$$

Consequently, in a sixty-second race, an average drag reduction of 2.1% could be expected to produce a 0.5-second reduction in elapsed time. Even a 0.4% reduction in drag could be expected to result in a 0.1-second drop in elapsed time. As discussed in Chapter 1, hundredths of seconds are significant in competition. Even taking into account that vortex generators would not be submerged over the entire race distance for all strokes, any drag reduction greater than 1% could be considered significant.

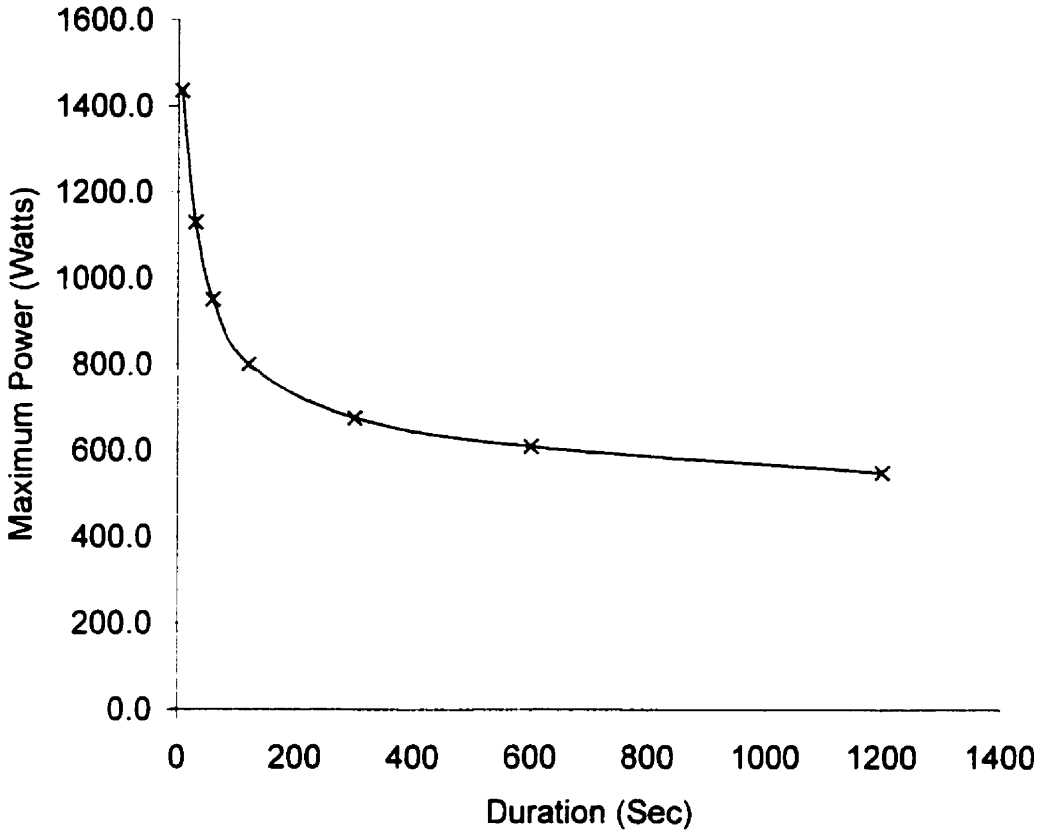

Figure 4.3: Maximum Human Power versus Duration (Adapted from Abbot and Wilson, 1995)

4.8.3 Vortex Configuration Codes

Due to the number of tested configurations, a coding system is required for concise classification. The code for each vortex configuration takes the following form:

R1-R2-R3-B-L-X-Y, where:

- R1 through R3 are the number of vortex generators in rows one to three respectively on the model's posterior,
- B is the number of vortex generators across the upper back,
- L is the number of vortex generators across the sides of the back, and

- X is distance, in inches, between the leading edge of the first row of vortex generators and the apex of the posterior as shown in figure 4.3.

- Y is the distance, in inches, between the leading edge of vortex generators mounted on the back and the apex of the posterior.

- A '0' in any code indicates that neither vortex generators nor fabric strips were used at that location while a '1' indicates that a fabric strip was used without vortex generators.

For example, the code, 20-12-0-1-12-1.25-9, describes a configuration with:

- 20 vortex generators in the first row (R1 = 20),

- 12 vortex generators in the second row (R2 = 12),

- Zero vortex generators in the third row (R3 = 0),

- A strip of fabric across the upper back (B = 1),

- 12 vortex generators (six on each side) across the sides of the back (L=12), and

- The leading edge of the first row of vortex generators was 1.25in forward of the apex of the posterior (X = 1.25).

- The leading edge of vortex generators on the back of the model are 9in forward of the apex of the posterior (Y = 9in).

This configuration is shown schematically in figure 4.4. The vortex generators are to scale relative to the model drawing. However, the vortex generators are shown as a two dimensional development. Consequently, they appear to extend beyond the sides of the model.

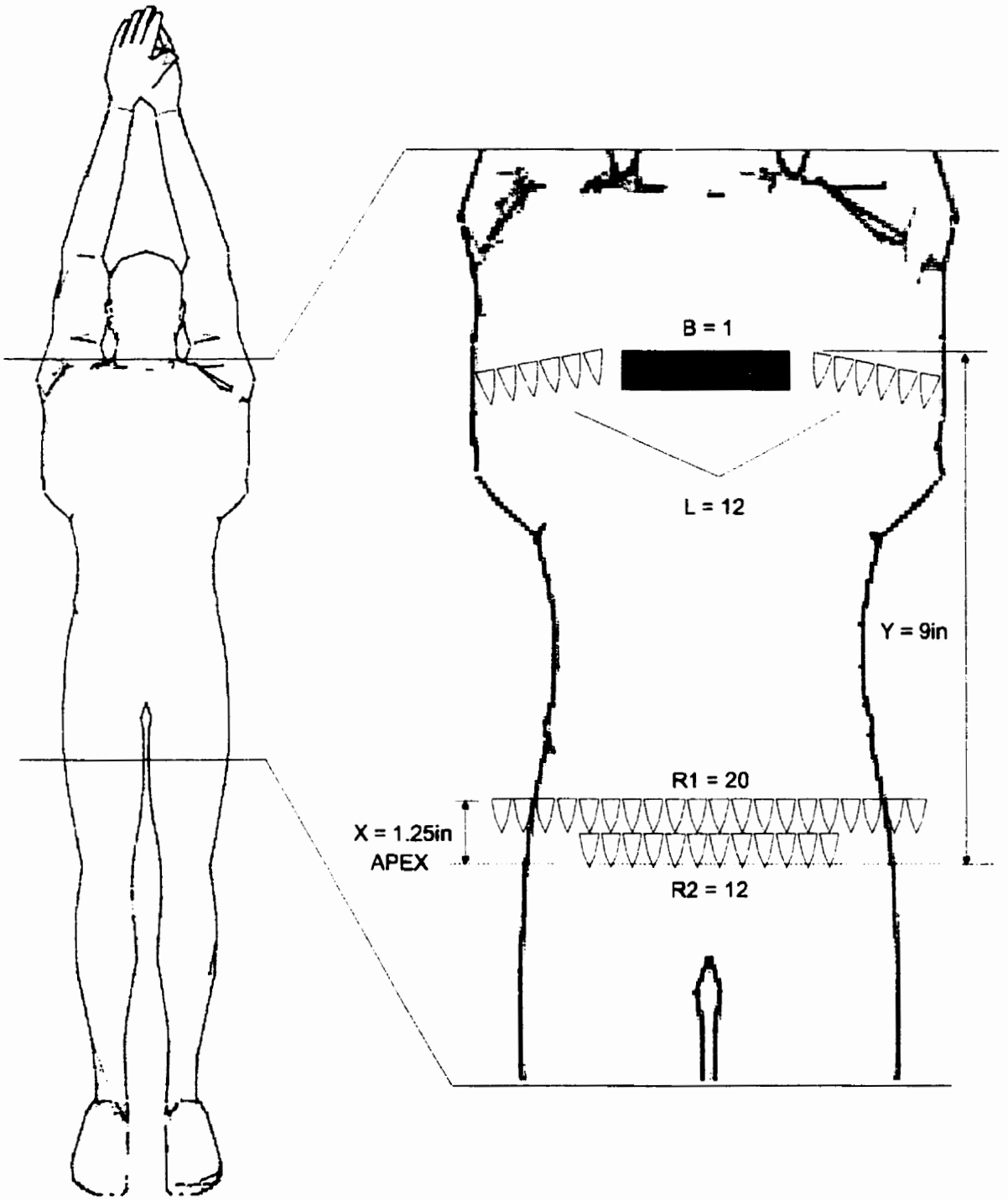

Figure 4.4: Vortex Configuration Code Example For 20-12-0-1-12-1.25-9

4.8.4 Stephens Vortex Generator Geometry

The geometry of the Stephens vortex generator array is based on a NACA inlet duct as described in RAS 66029 (1981) and is shown in figure 4.5. This geometry was scaled down for the model using the vortex generator height of 3mm as determined in section 4.7. The dimensions shown in inches, are those of the full-scale application.

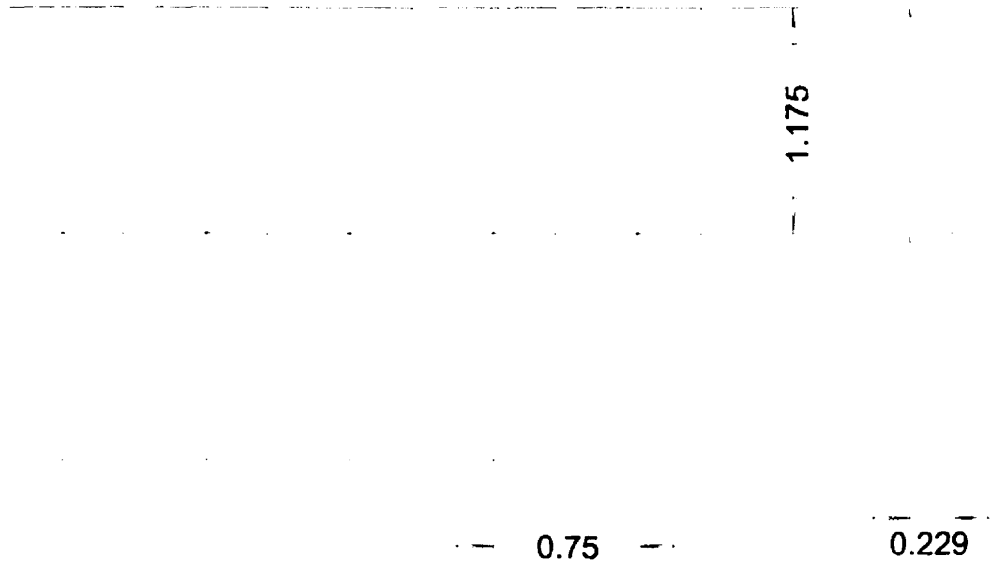

Figure 4.5: Stephens Vortex Generator Geometry (Dimensions in Inches)

4.8.5 Test Results for Fabric Mounted Stephens Vortex Generators

Figures 4.6 through 4.11 show the measured drag coefficients for various configurations within the constraints established in section 4.8.1. Figure 4.12 shows the various configurations together for comparison.

Figures 4.6 through 4.8 show configurations that include vortex generators on the posterior only. Various combinations of fabric strips and vortex generators were then affixed to the back of the model in an attempt to minimize the separation bubble in the small of the back.

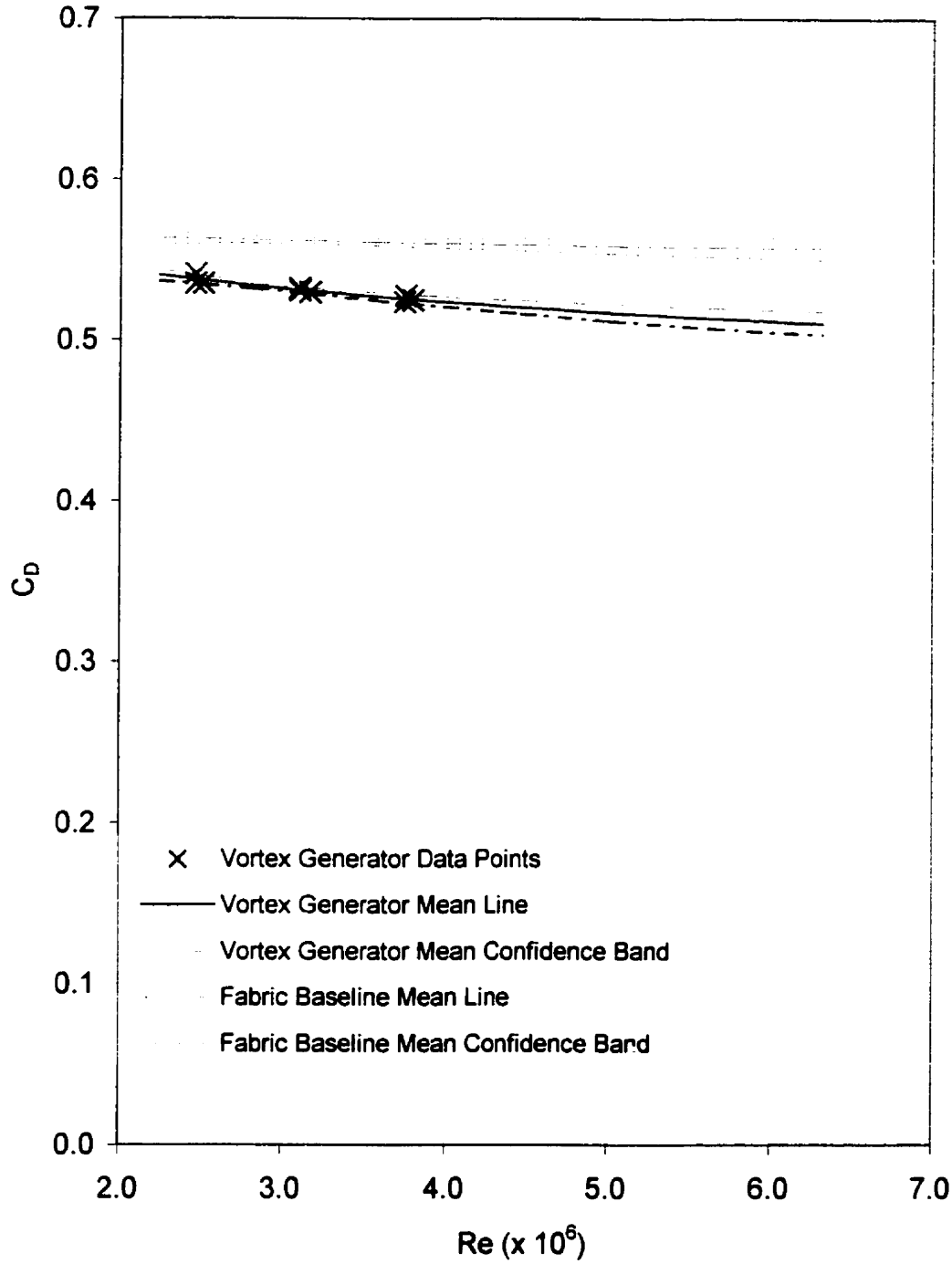

Figure 4.6: Drag Coefficient versus Reynolds Number for Fabric Mounted Stephens Configuration 20-0-0-0-0-1.25-0

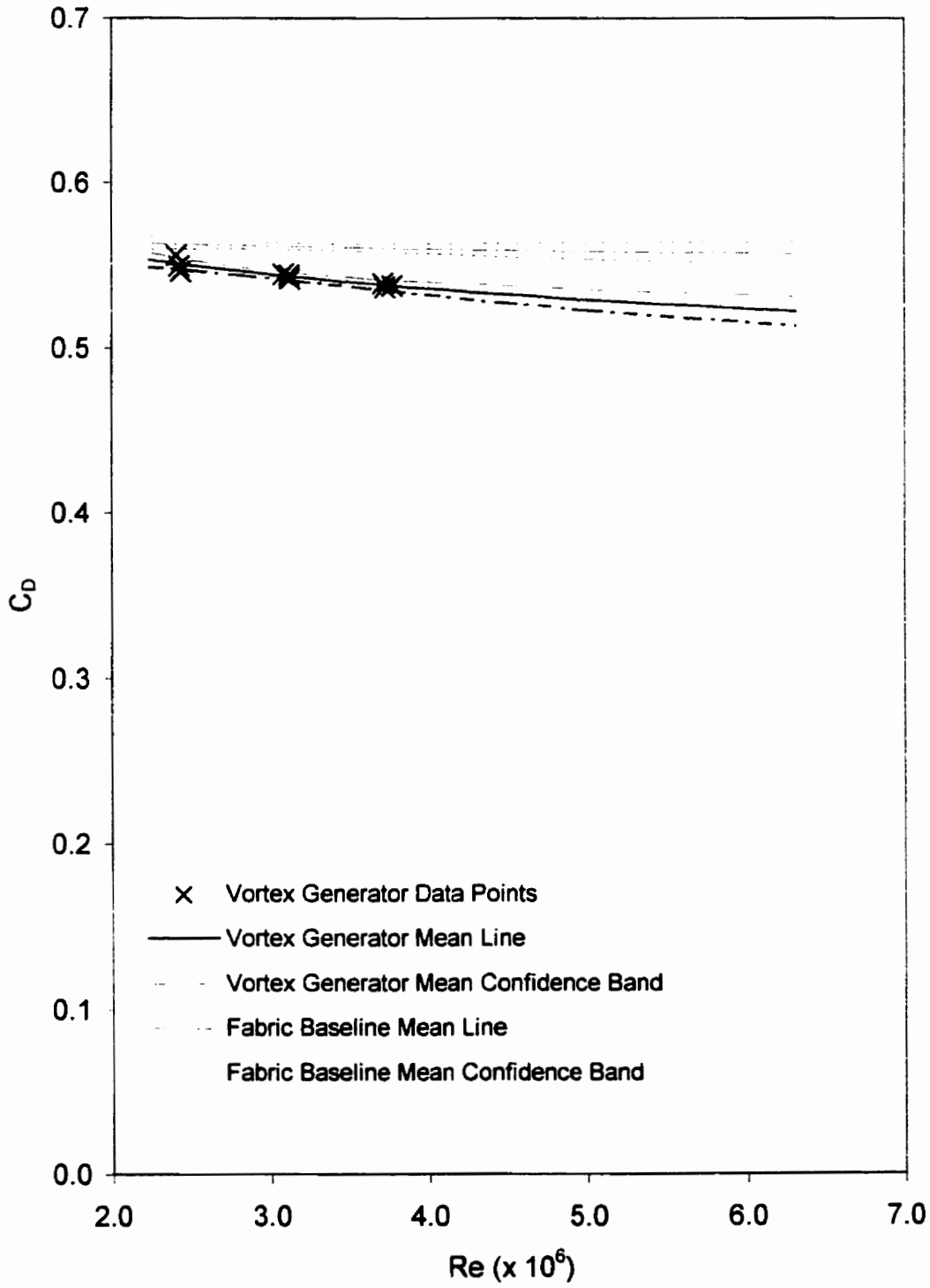

Figure 4.7: Drag Coefficient versus Reynolds Number for Fabric Mounted Stephens Configuration 20-12-0-0-0-1.25-0

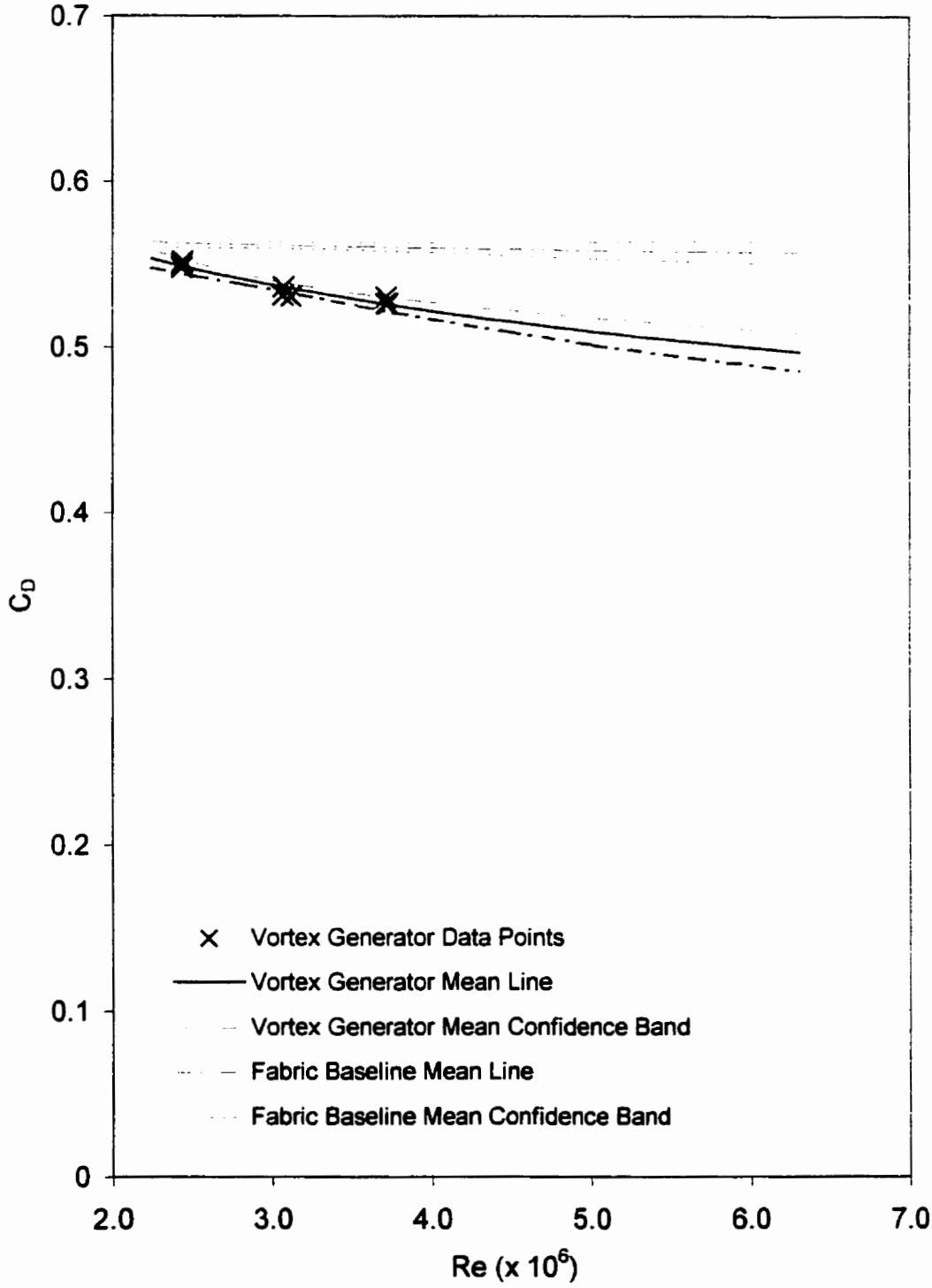

Figure 4.8: Drag Coefficient versus Reynolds Number for Fabric Mounted Stephens Configuration 14-12-0-0-0-0.75-0

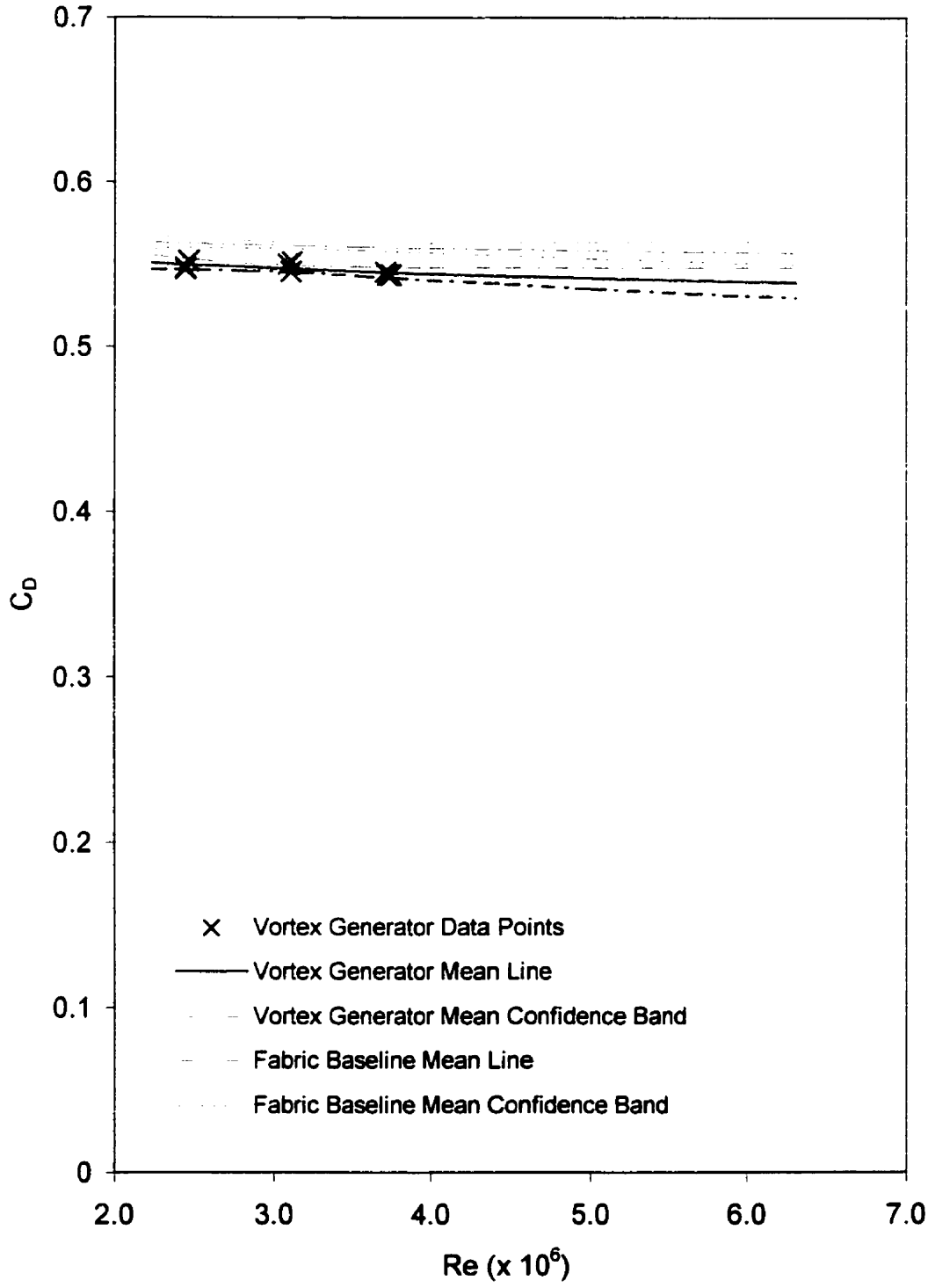

Figure 4.9: Drag Coefficient versus Reynolds Number for Fabric Mounted Stephens Configuration 20-12-0-10-12-1.25-9

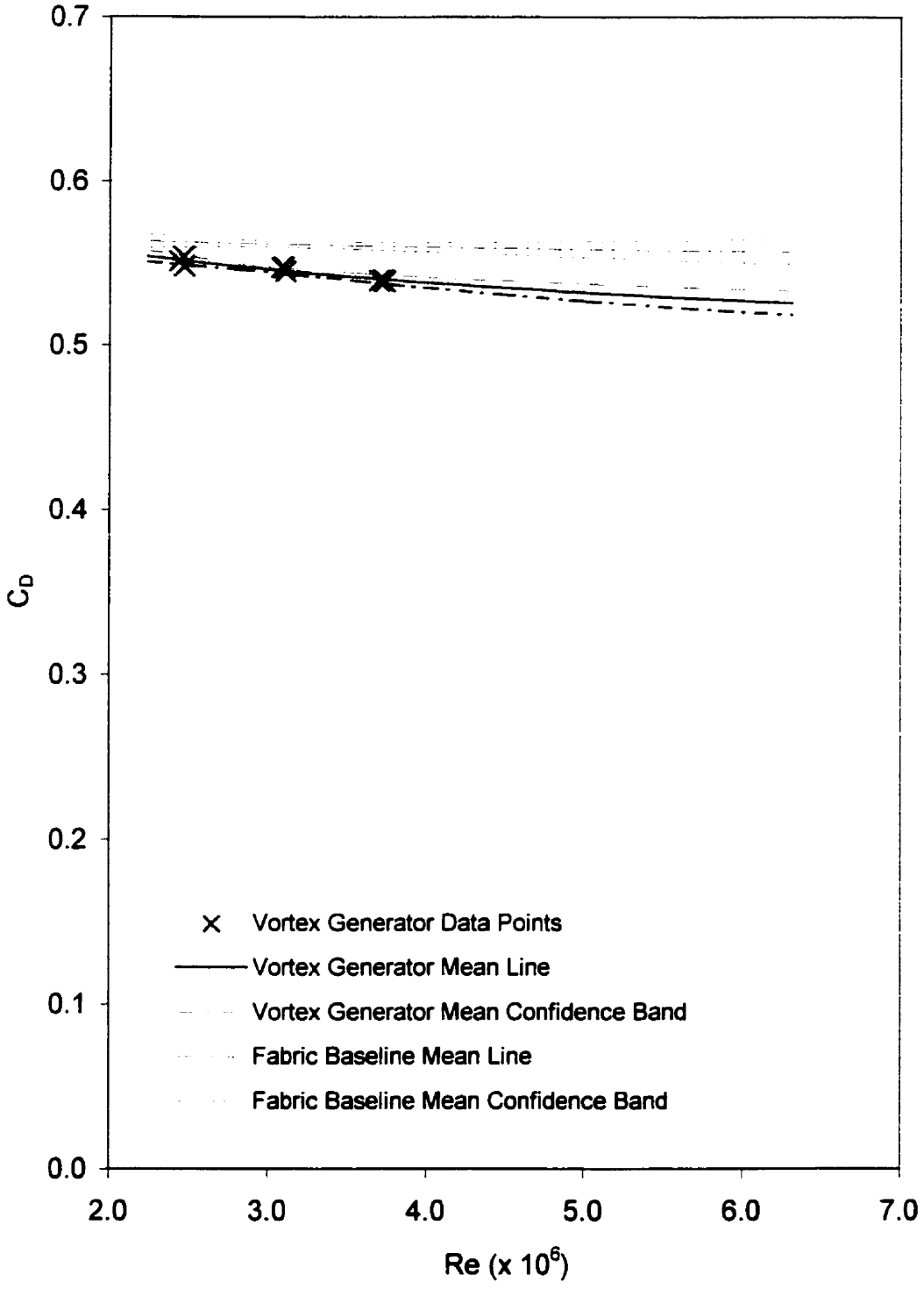

Figure 4.10: Drag Coefficient versus Reynolds Number for Fabric Mounted Stephens Configuration 20-12-0-10-12-1.25-7

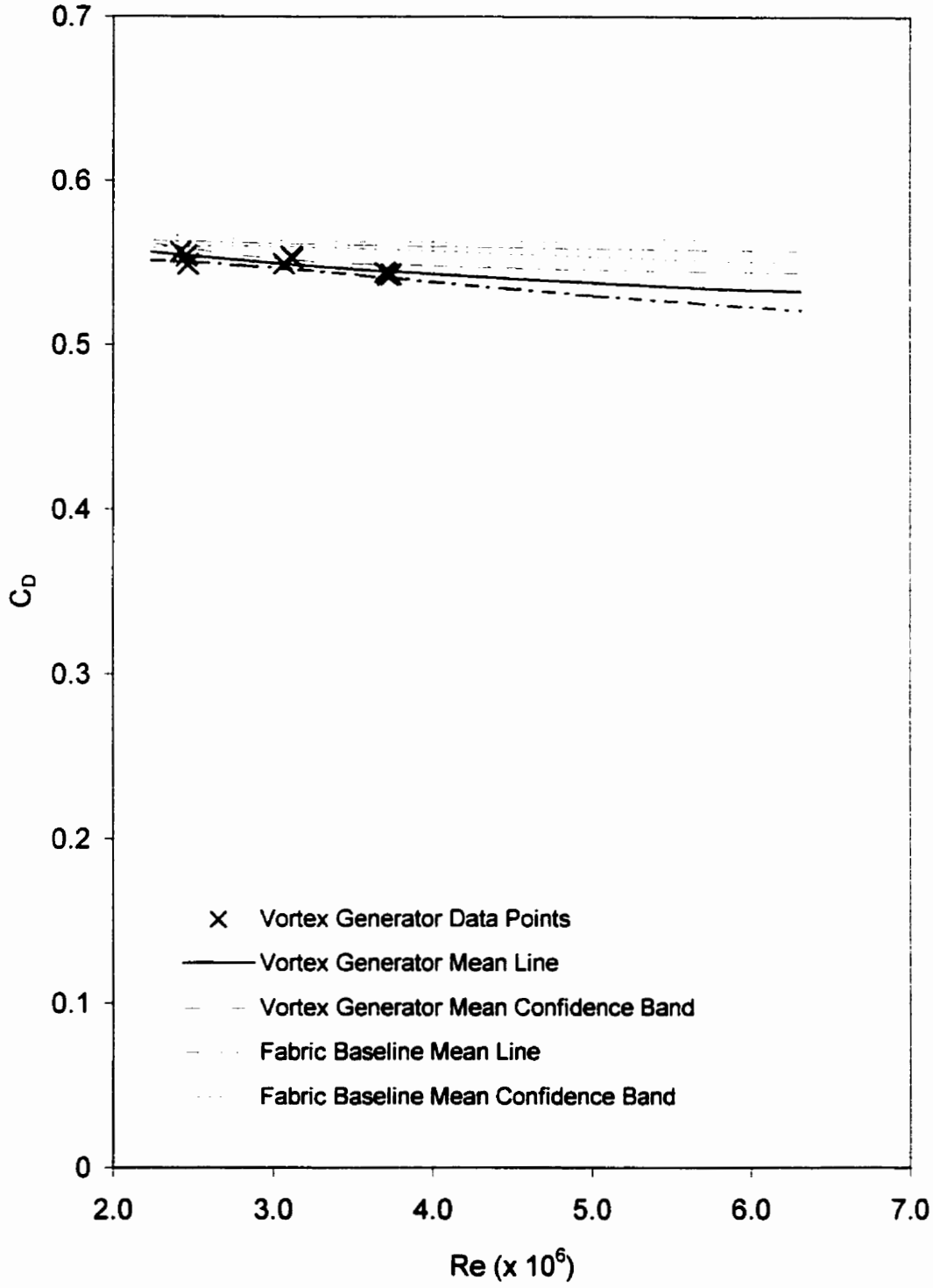

Figure 4.11: Drag Coefficient versus Reynolds Number for Fabric Mounted Stephens Configuration 20-12-0-1-12-1.25-9

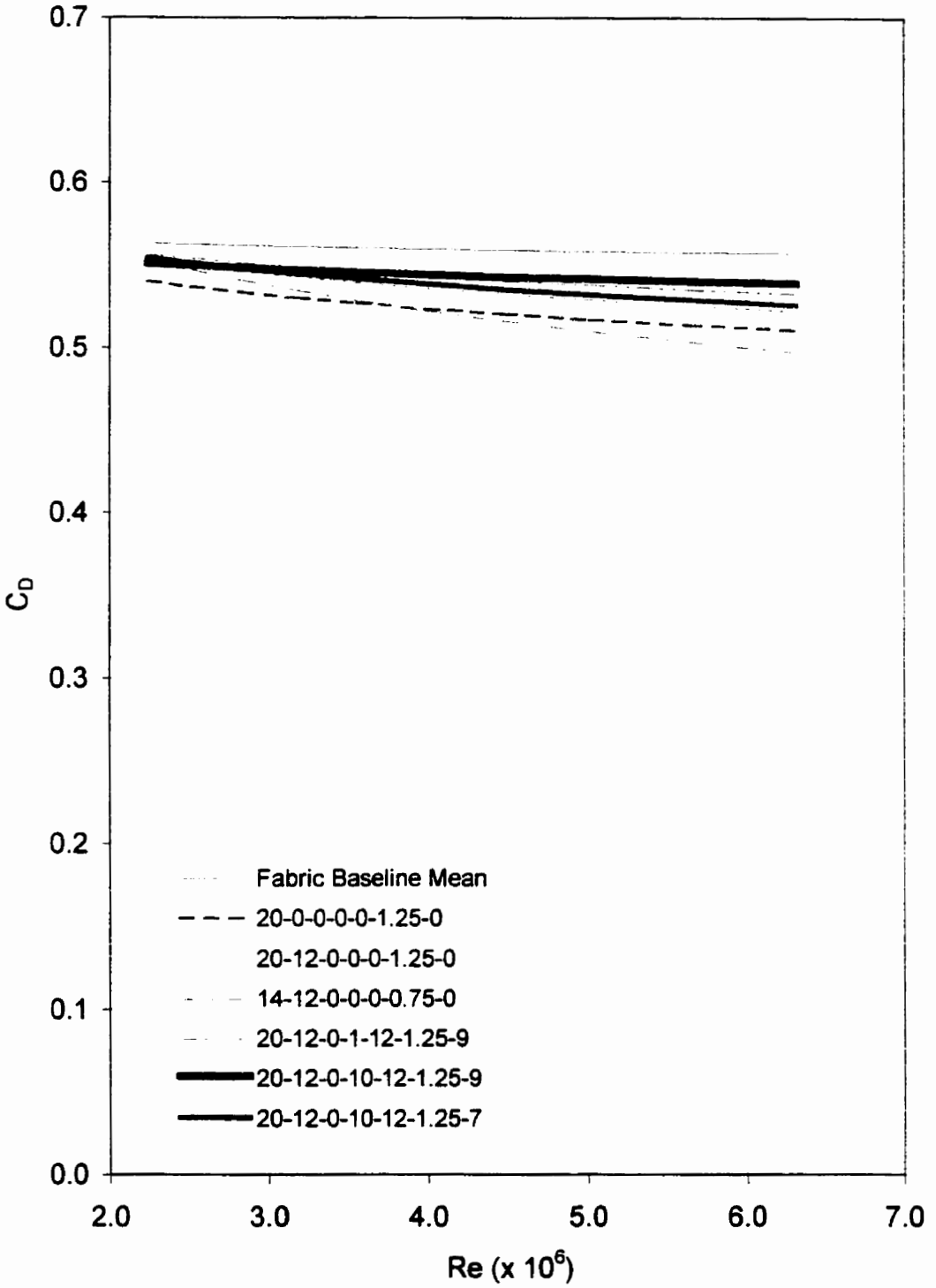

Figure 4.12: Drag Coefficient versus Reynolds Number Comparison for all Fabric Mounted Stephens Configurations

4.8.6 Discussion of Results for Fabric Mounted Stephens Vortex Generators

All of the fabric mounted Stephens vortex generator configurations showed a reduction in drag when compared with the baseline tests with fabric strips applied. The vortex generators also appeared to become more effective with increasing Reynolds number.

The two most promising configurations, 20-0-0-0-0-1.25-0 and 14-12-0-0-0-0-0.75-0, each showed a drag reduction of approximately 6% at a Reynolds number of 3.75×10^6.

The application of either fabric strips or vortex generators to the upper back of the model offered no apparent reduction in drag. No attempt was made to alter the size of the vortex generators to account for the thinner boundary layer upstream. Consequently, the size of the vortex generators was probably not optimal for reducing the size of the separation bubble in the lumbar region of the back. In addition, the separation bubble in the small of the back was observed to be smaller than the posterior one. This suggests that the posterior separation bubble is a larger contributor to overall drag than the lumbar one. Consequently, no subsequent testing was conducted with vortex generators affixed to the model's back.

4.8.7 Test Results for Directly Mounted Stephens Vortex Generators

The method of testing was modified to permit more expedient screening of potential vortex generator configurations. The vortex generators were affixed to the model by means of double-sided tape. Since the fabric was eliminated, all testing reported hereafter is compared to the clean baseline.

Tests of the various directly applied Stephens vortex generator configurations shown in figures 4.13 through 4.16 generally include three data points. The intention was to go back and retest configurations that showed the most promise for drag reduction. However, as will be discussed in the following section, feedback from real-world users forced the abandonment of the Stephens type vortex generator in favour of the Kuethe type. Figure 4.13 shows the four configurations that were tested with the first row of vortex generators 1.25in upstream of the apex of the posterior. Figures 4.14 through 4.16 show the test results for various configurations for X = 0.75in. These results were grouped into three sets in order to alleviate the visual clutter that would have resulted if they were all shown on the same graph.

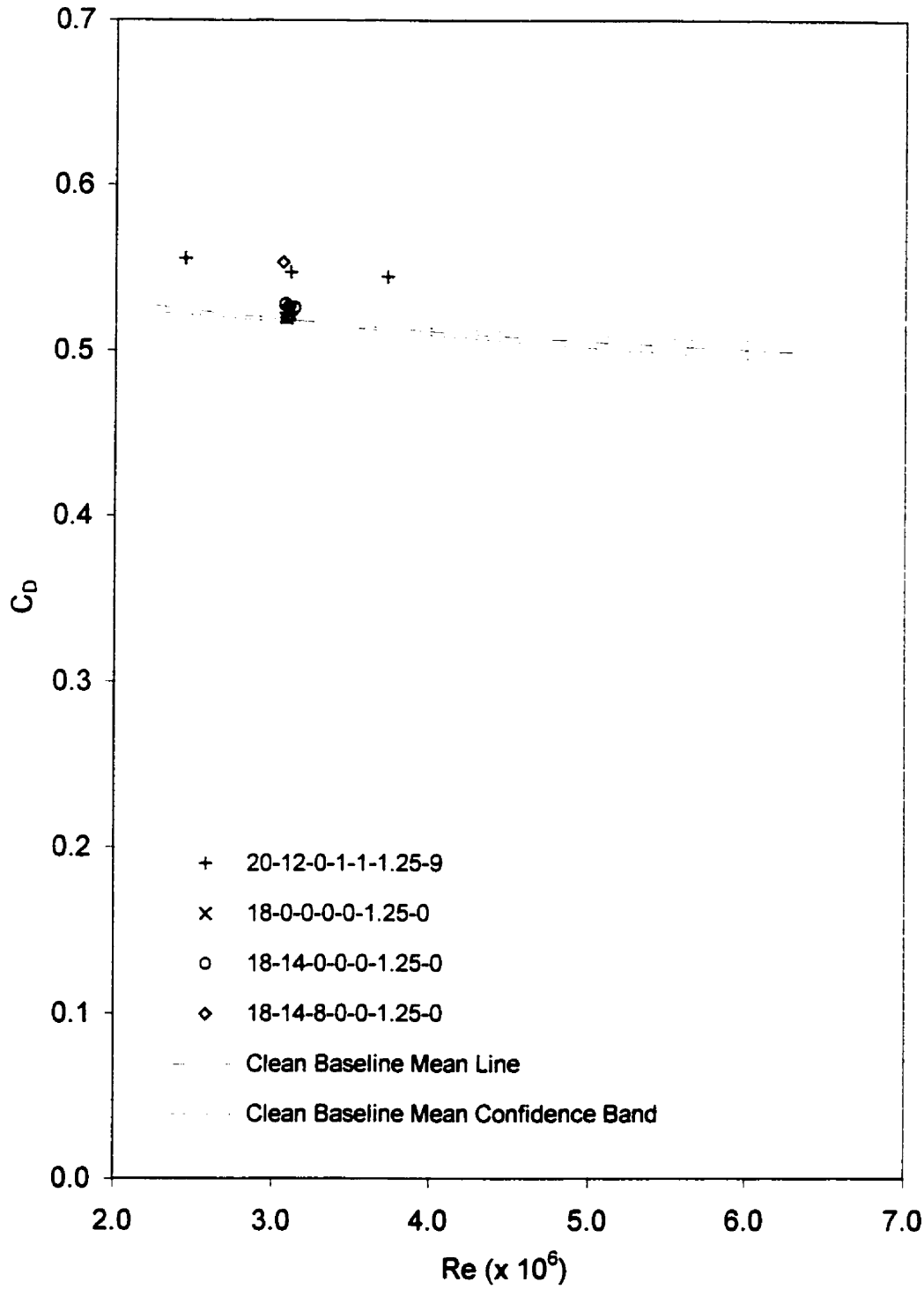

Figure 4.13: Drag Coefficient versus Reynolds Number for Directly Mounted Stephens with X = 1.25in

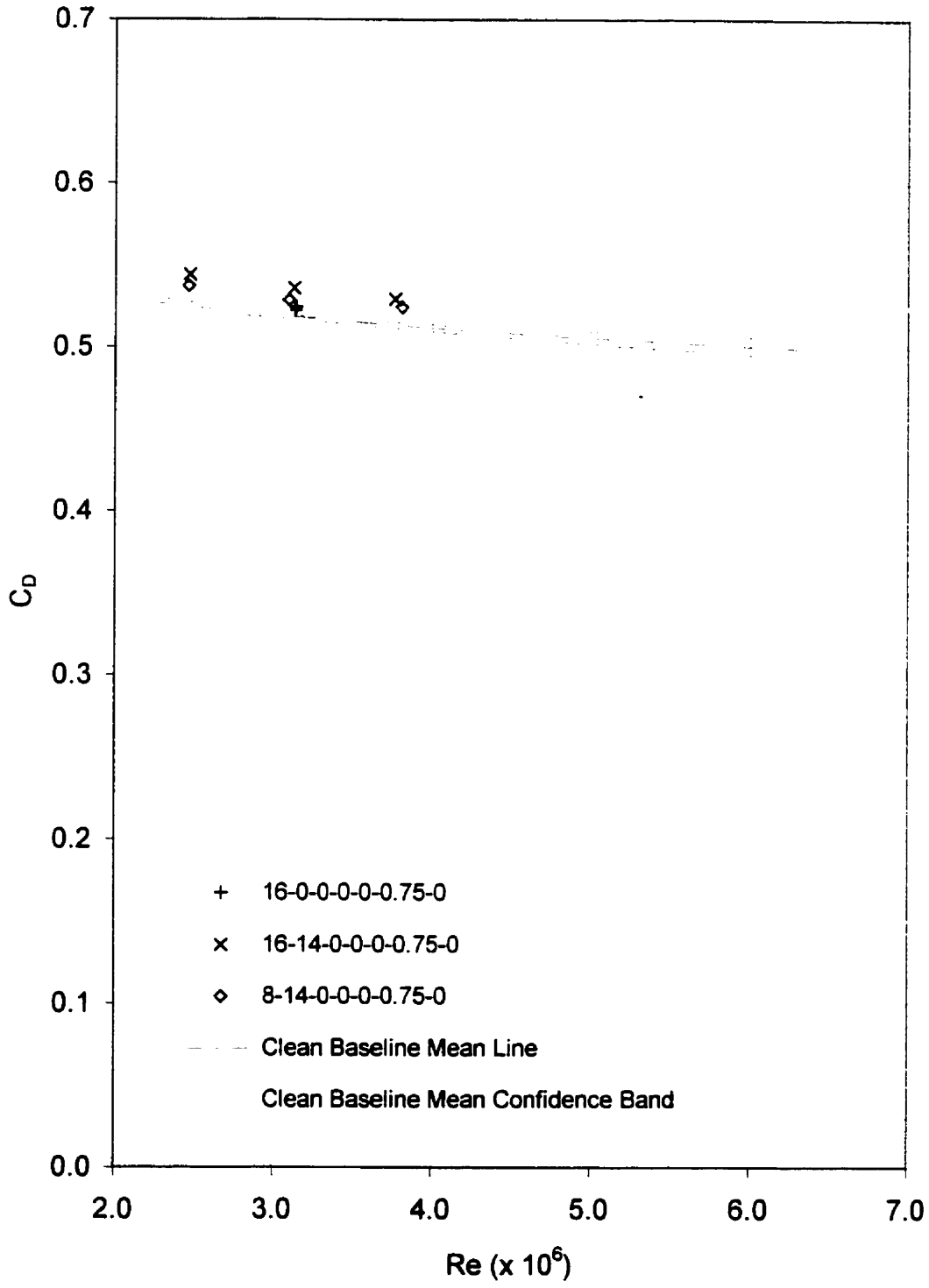

Figure 4.14: Drag Coefficient versus Reynolds Number for Directly Mounted Stephens Test with X = 0.75, Set 1

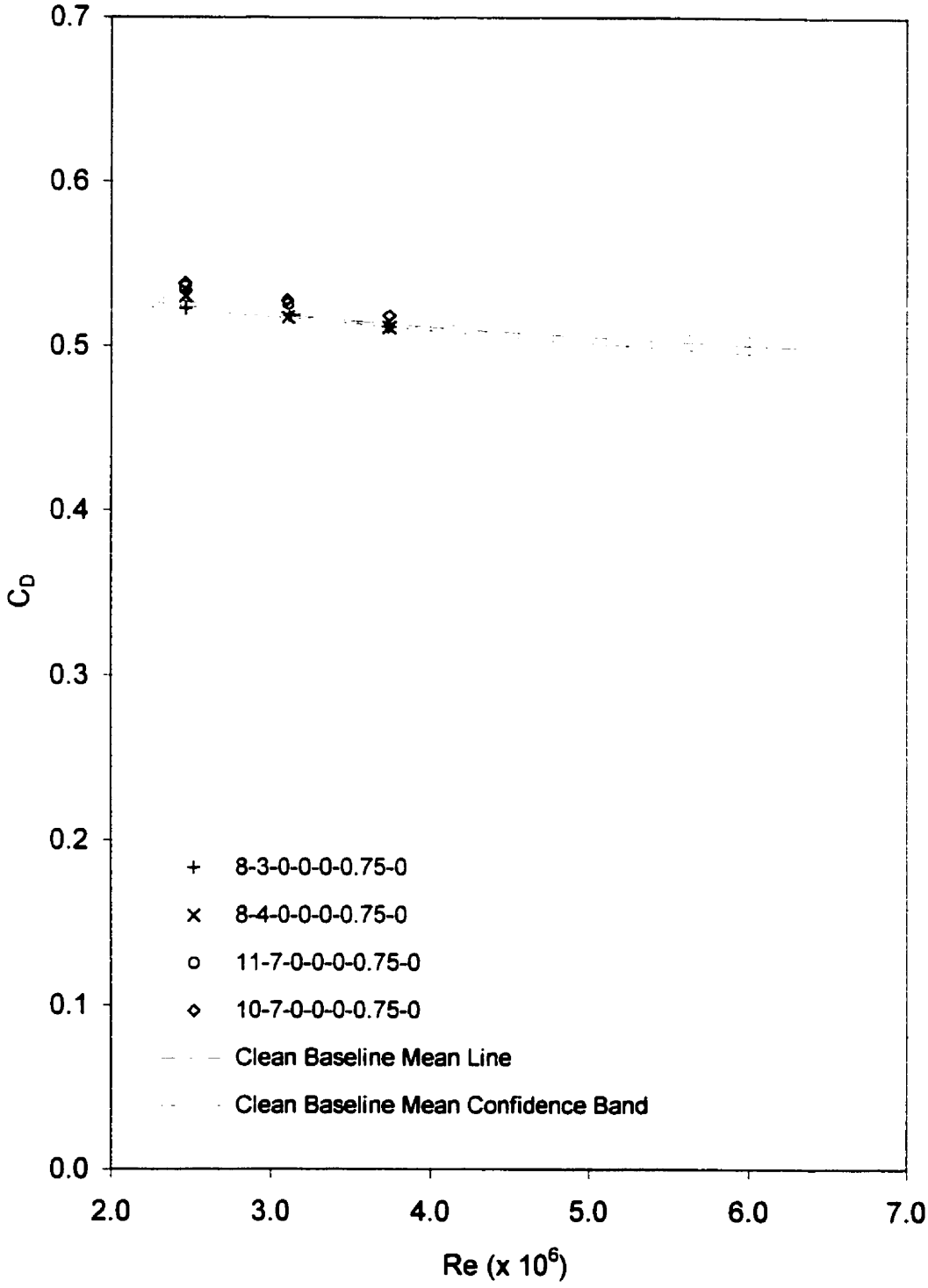

Figure 4.15: Drag Coefficient versus Reynolds Number for Directly Mounted Stephens Test with X = 0.75, Set 2

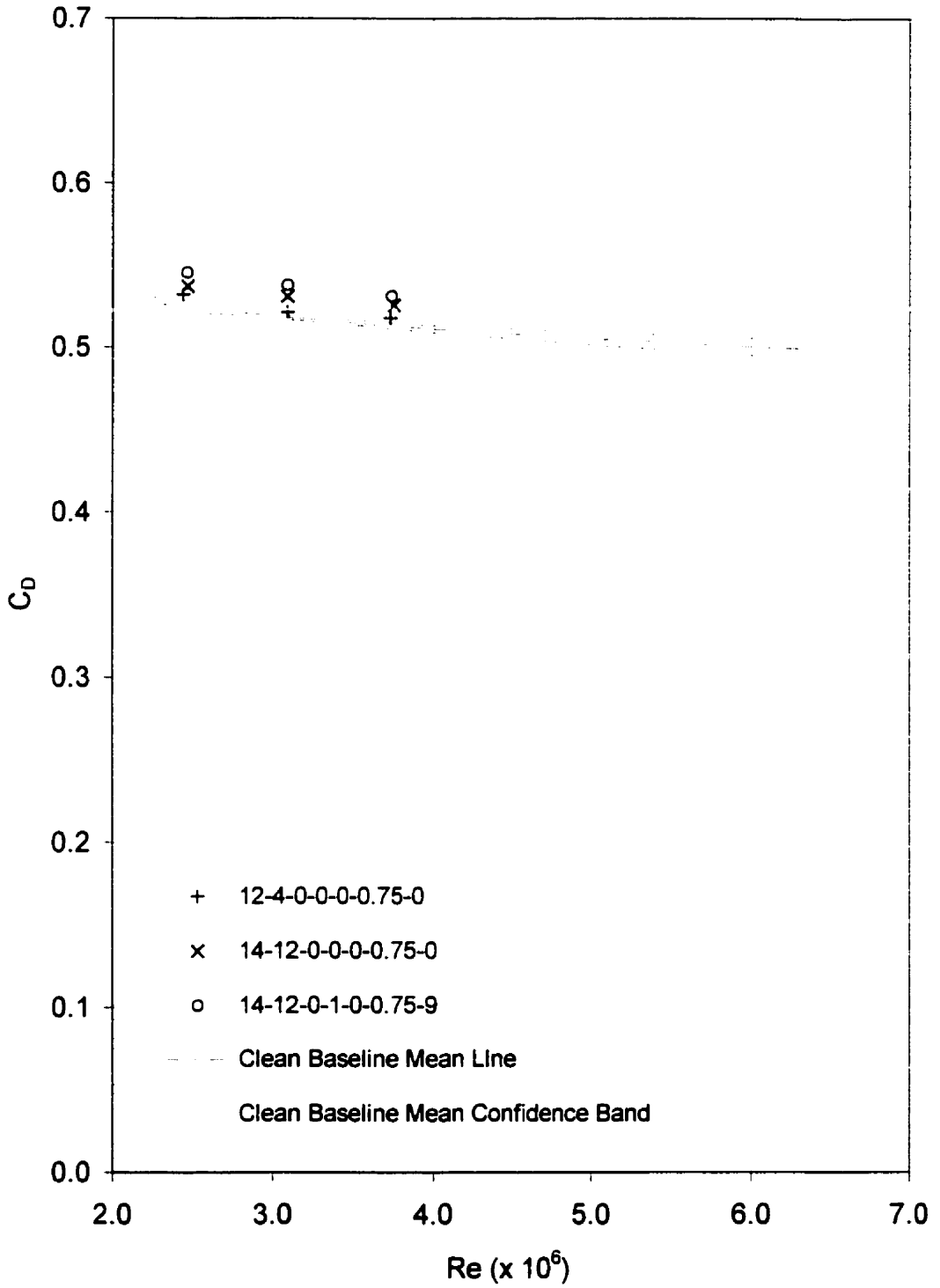

Figure 4.16: Drag Coefficient versus Reynolds Number for Directly Mounted Stephens Test with X = 0.75, Set 3

4.8.8 Discussion of Results for Directly Mounted Stephens Vortex Generators

Generally, none of the directly mounted Stephens vortex generator configurations exhibited a reduced drag coefficient when compared with the clean baseline. However, the 8-4-0-0-0-0.75-0 configuration broke even. This implies that the vortex generator device drag for this configuration was equal to the reduction in drag resulting from delayed separation.

The 16-14-0-0-0-0.75-0 configuration shown in figure 4.14 appeared to eliminate the separation bubble. This conclusion was based on observation of the tufts immediately downstream of the posterior. These tufts were observed to be lying flat against the model surface and to be pointing aft. This contrasts with the overall drag increase for this configuration in comparison with the clean baseline. This implies that the device drag of this particular vortex generator configuration was greater than the drag generated by the separation bubble. This, in turn, suggests that a more optimal configuration may employ smaller vortex generators with lower drag coefficients.

Based on the results of the fabric-mounted testing, swimsuits fitted with Stephens vortex generators had been used in competition. The suits were successful in Masters' swimming with several Canadian national titles being won and a Masters' national record being set. However, when initially introduced to members of the US National Team, the weight and aesthetics of the suit were found unacceptable. The points of the Stephens vortex generators tended to catch when sitting, thus causing them damage. Consequently, testing of the Stephens vortex generators was discontinued and a more practical design was sought.

4.9 Kuethe Vortex Generators

The Kuethe vortex generator, described in chapter 2, has a constant height with no sharp edges. This, it was anticipated, would make the vortex generators less susceptible to damage during real-world use.

The Kuethe type was tested without fabric backing in order to remove its interaction with the vortex generators. In addition, it was desirable to demonstrate a drag reduction under the apparently more conservative clean conditions. This, it was hoped, would increase confidence that the drag reductions observed for the fabric mounted vortex generators were not merely an artefact of the interaction between the fabric and the vortex generators.

4.9.1 Test Results for Type 1 Kuethe Vortex Generators

The Type 1 Kuethe vortex generators, shown in figure 4.17, were created by printing a series of capital Vs with a Dymo-labeller. The dimensions shown in figure 4.17 are those of the vortex generators affixed to the model. The adhesive backing and the regularly shaped and spaced Vs made this a particularly convenient and repeatable arrangement. The height of the type 1 Kuethe vortex generators was approximately 0.05δ. This is below the minimum recommended height of 0.1δ suggested by Lin et al (1990). However, since the value of δ estimated for the model is probably high as discussed in section 4.7.1, the low height of the Type 1 Kuethe vortex generators might still be effective. In any case, a shorter height seemed appropriate given that the results for the 0.25δ Stephens vortex generators suggested they might have been higher than required. Figure 4.18 shows the results of testing for two configurations of Type 1 Kuethe vortex generators.

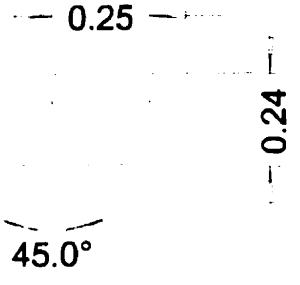

Figure 4.17: Type 1 Kuethe Vortex Generators (Dimensions in Inches)

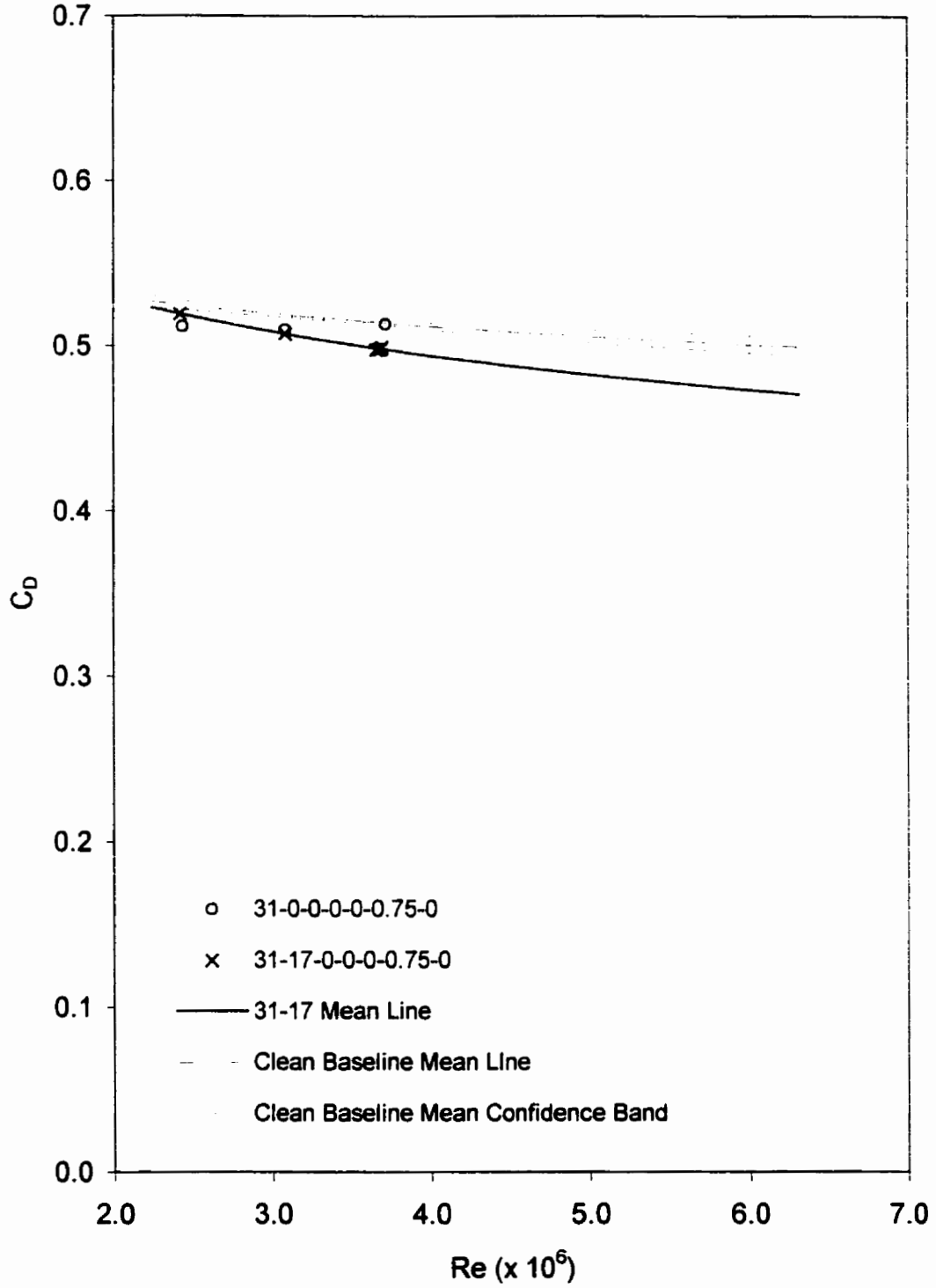

Figure 4.18: Drag Coefficient versus Reynolds Number for Type 1 Kuethe Vortex Generators.

4.9.2 Discussion of Results for Type 1 Kuethe Vortex Generators

Figure 4.18 indicates that the single row of vortex generators became less effective with increasing Reynolds Number. Conversely, the measured improvement in drag coefficient for the double row of vortex generators increases with higher Reynolds numbers. The small vortices produced by the Type 1 Kuethe vortex generator may have a short persistence. The second row may have served to reinforce the vortices created by the first row. This would allow the vortices to persist downstream of baseline separation. At the lowest tested speeds, the boundary layer immediately upstream of the vortex generators may not yet have been fully turbulent. Consequently, the single row would have served to trip the boundary layer at these lower Reynolds numbers. This would have delayed separation and accounted for the single row's effectiveness at lower Reynolds numbers.

4.9.3 Test Results for Type 2 Kuethe Vortex Generators

The geometry of the Type 1 Kuethe vortex generators was inherently arbitrary and not necessarily optimal. In addition, the manufacturing technique for the end application entailed individually moulding and bonding each vortex generator to a swimsuit. Consequently, the 48 vortex generators, required by the best Type 1 configuration, would have required excessive labour to manufacture with the techniques available.

Consequently, a larger set of Kuethe vortex generators was tested with a height of 0.1δ. The included angle of the vortex generator was reduced to 30°. This is in line with the 15° angle of attack recommended by Kuethe (1972). Figure 4.19 shows the dimensions for the full-sized Type 2 Kuethe vortex generator as used in competition.

The Type 2 Kuethe vortex generators were initially tested in four configurations. These consisted of either a single row of 10 vortex generators or two rows with 10 in the first and eight in the second. Each of these configurations was tested at 0.75in and 1.0in ahead of baseline separation initiation. Of the initially tested configurations, the 10-8-0-0-0-0.75-0 configuration showed the most promise and was tested more extensively. The results of this testing are shown in figure 4.20. The test results for the other three configurations are shown together in figure 4.21.

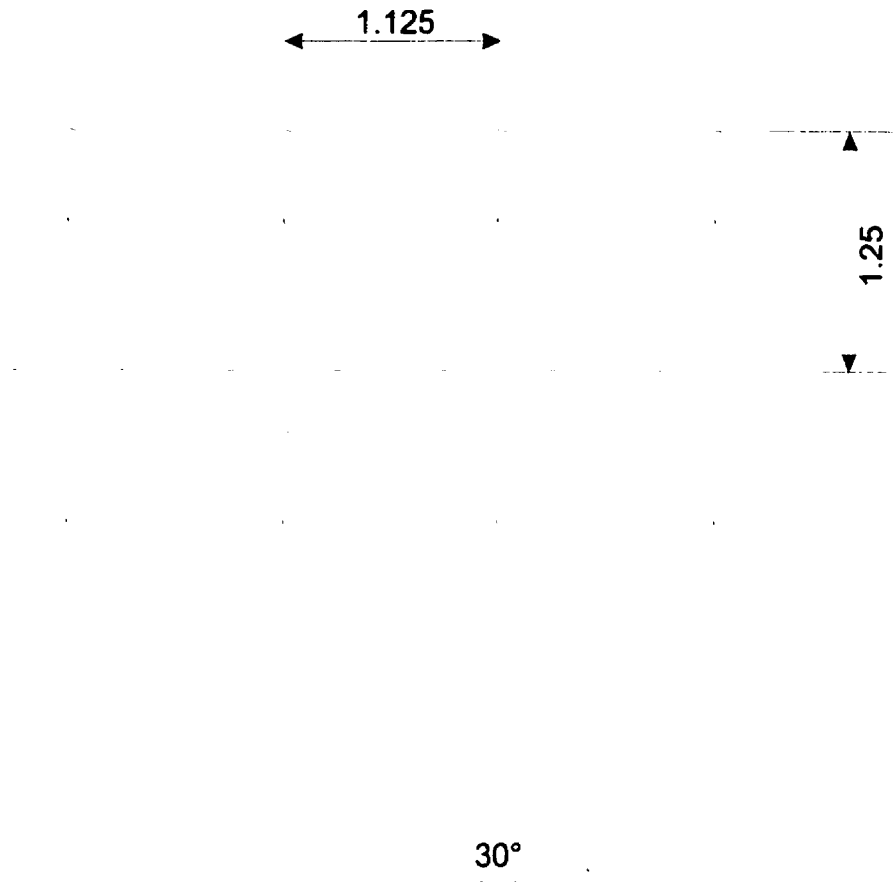

Figure 4.19: Type 2 Kuethe Vortex Generators (Dimensions in Inches)

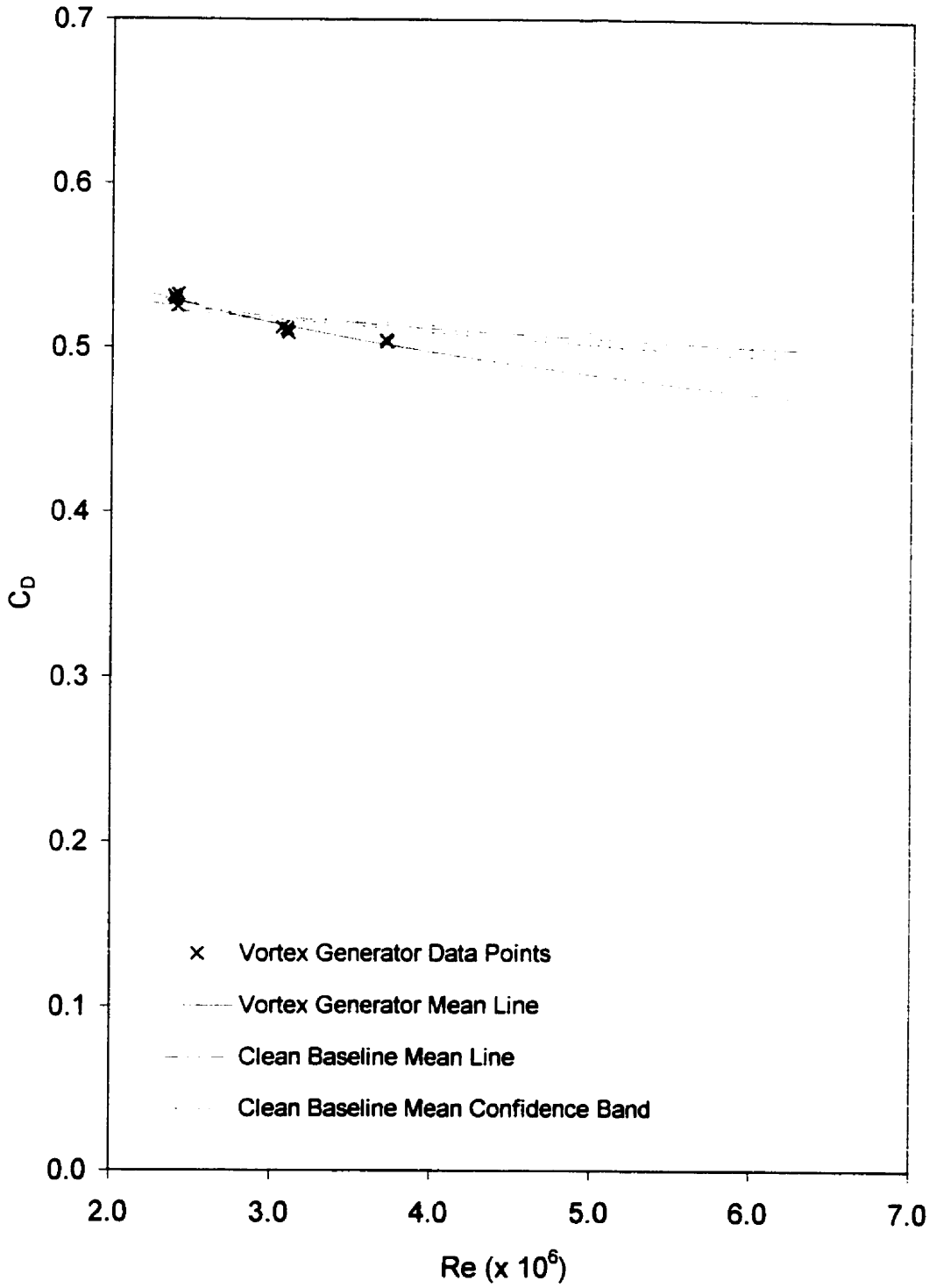

Figure 4.20: Drag Coefficient versus Reynolds Number for Type 2 Kuethe Vortex Generator Configuration 10-8-0-0-0-0.75-0.

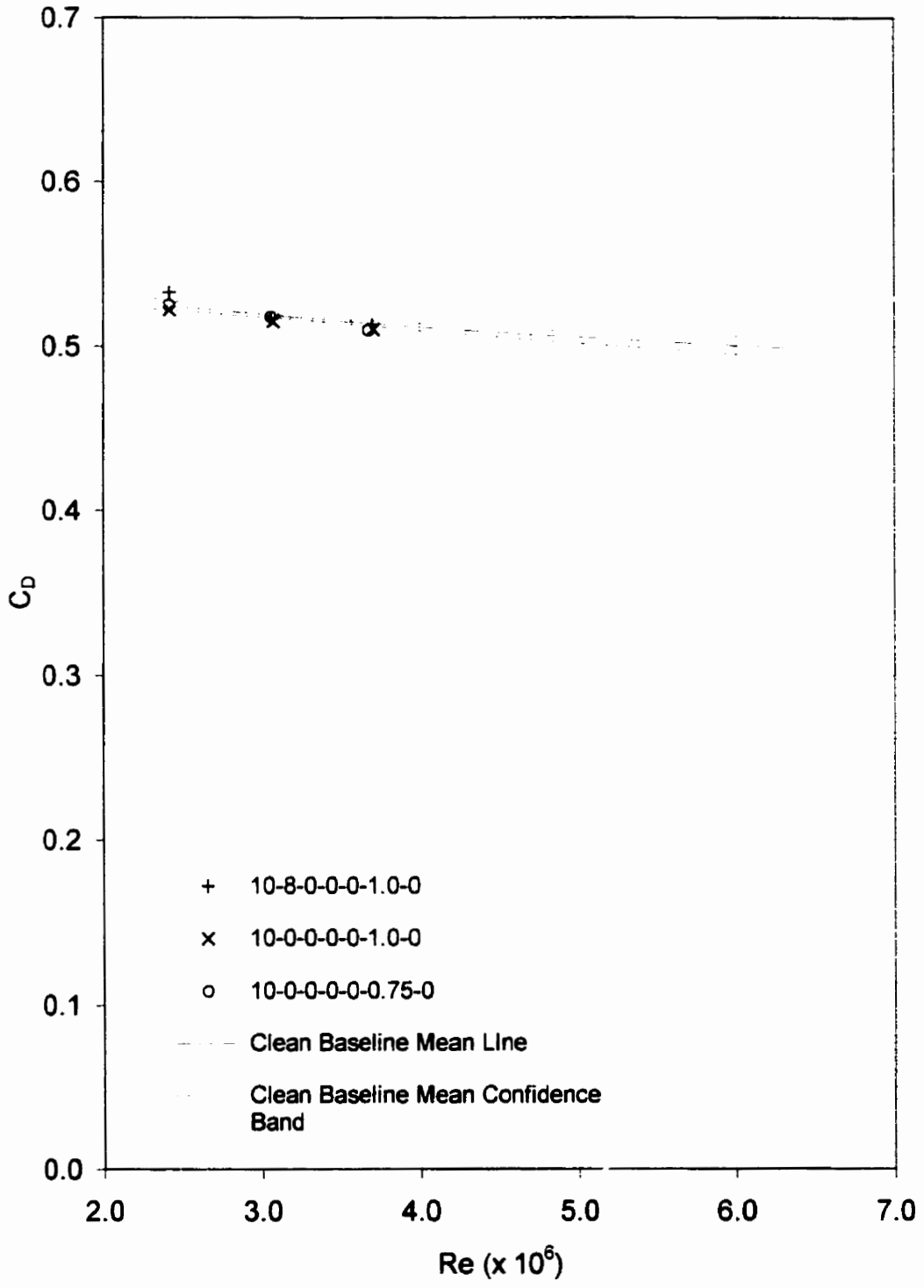

Figure 4.21: Drag Coefficient versus Reynolds Number for other Type 2 Kuethe Vortex Generator Configurations.

4.9.4 Discussion of Results for Type 2 Kuethe Vortex Generators

The 10-8-0-0-0-0.75-0 Type 2 Kuethe configuration showed a drag reduction of approximately 2% at Reynolds numbers above 3.0×10^6. As discussed in section 4.8.2 this amount of drag reduction could be expected to reduce a swimmers elapsed time in a 100-metre race by several tenths of a second. Assuming that Kuethe vortex generators interact with swimsuit fabric in the same manner as that observed for the Stephens type in section 4.8, the true drag reduction could be greater.

Jenny Thompson of the USA first used the Type 2 Kuethe vortex generators in a major competition at the 1996 Olympics in Atlanta where she won three gold medals. Her split time of 58.53 seconds for the butterfly leg of the 4 x 100m medley relay was the second fastest ever recorded. More recently, at the 1999 Pan Pacific Championships in Sydney Australia, Jenny Thompson and Lenny Krayzelburg combined to establish four new world records while wearing Type 2 Kuethe vortex generators. Ms. Thompson set a new standard in the 100m Butterfly while Mr. Krayzelburg set new world records in the 50m, 100m, and 200m backstroke races. These successes at least anecdotally support the test results.

5 CONCLUSIONS AND RECOMMENDATIONS

5.1 Applicability of Results to Swimmer

5.1.1 Static Test vs. Moving Swimmer

The static tests conducted in this study are directly applicable only to a swimmer who is not moving their arms or legs. This condition does occur in a race immediately following a turn or start. However, as soon as the swimmer starts kicking and pulling, the flow around their body becomes dynamic and unsteady. In addition, any analysis of surface swimming must take into account the effect of the air-water interface.

Despite the tendency for swimmers to remain submerged as long as the rules will allow, surface swimming still comprises the majority of most swimming races. Consequently, there is a need to measure the influence of various drag reduction techniques during this phase of the race.

5.1.2 Air Vs. Water

Air and water are both Newtonian fluids and each has been used in testing to predict flow in the other. Matching the Reynolds numbers (the most relevant parameter for the submerged swimmer) in the two media should tend to give the same overall flow patterns and drag coefficients. This correlation could be confirmed by testing the same model in both an air and water tunnel at the same Reynolds number.

5.1.3 Reynolds Number Variation

The maximum test velocity of 46.5m/s corresponds to a Reynolds number of 3.75×10^6. The range of Reynolds numbers for world class swimmers, as discussed in section 4.1.2, is approximately 3.0×10^6 to 6.3×10^6. Consequently, the range of Reynolds numbers for the test data intersects that for elite swimmers. However, it would be prudent to perform tests at higher velocities in order to confirm the effectiveness of vortex generators across the entire range of interest.

5.2 Significance of Results

As shown in section 4.8.2, a drag reduction of 2.1% could be expected to lower 100-metre times by 0.5 seconds. Consequently, the measured drag reductions of 2% for the Type 2 Kuethe and 6% for the fabric mounted Stephens vortex generators could be expected to drop several tenths of a second off a 100-metre race. To illustrate the significance of this, one notes that Daichi Suzuki of Japan won the 1988 Olympic 100 metre backstroke in a time of 55.05 seconds while Sergei Zabolotnov of Uzbekistan, who finished in 55.37 seconds, was fourth.

5.3 Future Static Testing Recommendations

5.3.1 Change model mounting method

The three point mounting method allowed too much vibration in pitch and yaw during testing. This prevented reliable measurement above sixty percent of the wind tunnel's maximum air velocity. In addition, the three-point mount introduced significant tare drag.

Future testing should be conducted with a single, centrally mounted strut. This will constrain the model in pitch and should cut down on flutter. The increased torsional stiffness of a single robust strut should also prevent model vibration in yaw at higher speeds. In addition, the single strut should reduce the total tare drag.

5.3.2 Improve Anthropomorphism

An early version of Poser software was used, in part, to create the wind tunnel model. This software had limited choices for body types and tended to produce idealized forms. In practical terms, this meant the model had a large chest and narrow hips. While some elite swimmers may approach this form, it is probably not representative of the majority.

The smaller hip area of this model may have led to a smaller separation bubble downstream of the posterior. This ultimately may have lead to an underestimate of its overall drag contribution. The latest version of Poser is able to produce a variety of more realistic body types. A model created with this software should more accurately model the drag contribution from the posterior.

5.3.3 Alter Arm Position

The angled arm position was intended to be a more realistic representation of an achievable posture. This was based on observing the best arm position of a number of competitive swimmers. However, further observation of submerged elite swimmers has shown that they are able to achieve an ideal straight-arm position. Assuming this improved posture reduces overall drag, the relative drag contribution of the posterior separation bubble would probably increase.

5.4 Proposed Dynamic Testing through Measurement of Heartbeats per Lap

This test method would involve recording the number of heartbeats per lap for a swimmer and plotting this against the time taken for each lap. If the swimmer's velocity is steady and their effort level is below the anaerobic threshold, the number of heartbeats on a given lap should be related to the energy expended for that lap.

This method would not give a direct measure of drag or energy consumption. However, for a given swimmer it could be used to compare the effort level wearing two different swimsuits.

Clearly, the experiment would require psychological controls in order to have a meaningful result. Since this method uses an actual swimmer, in a pool, with minimal equipment, it could prove useful in discriminating between suit designs.

5.5 Computer Modelling

Since this thesis was first planned, computers have become four times faster for the same cost. At the same time, human modelling software has become more anatomically accurate. Consequently, it should now be cost-effective to model vortex flow on a submerged swimmer using computational fluid dynamics (CFD). Such a study would provide excellent flow visualization. In addition, it may be able to optimize the vortex generator configuration with greater precision than is possible with experimental techniques.

References

Abbott, V.A. and Wilson, D.G. 1995. *Human-Powered Vehicles*. Human Kinetics, Champaign, IL.

Barlow, J.B., Rae, Jr.,W.H. and Pope, A. 1999. *Low-Speed Wind Tunnel Testing*, Third Edition. John Wiley & Sons, Inc., New York, NY.

Clarys, J.P. 1978. "An Experimental Investigation of the Application of Fundamental Hydrodynamics to the Human Body". 4th International Congress on Swimming Medicine. Pages 388-394. University Park Press, Baltimore, MD.

Clarys, J.P. 1979. "Morphology and Hydrodynamics". 3rd International Symposium of Biomechanics in Swimming. Pages 3-44. University Park Press, Baltimore, MD.

Gross, A.C., Kyle, C.R. and Malewicki, D.J. 1983. "The Aerodynamics of Human-Powered Land Vehicles" Scientific American, December. Pages 142-152. Scientific American Inc., New York, NY.

Hollander, A.P., Groot, G. de, Ingen Schenau, G.J. van, Toussaint, H.M., Best, H., de, Peeters, W., Meulmans, A. and Schreurs, A.W. 1986. "Measurement of Active Drag Forces During Swimming". Journal of Sport Sciences. Volume 4. Pages 21-30.

Holmér, I. 1974. "Energy Cost of Arm Stroke, Leg Kick And The Whole Stroke In Competitive Swimming Styles". European Journal of Applied Physiology. Volume 33. Pages 95-103.

Kraemer W.J., Bush, J.A., Bauer, J.A., Tripplet-McBride, N.T., Paxton N.J., Clemson, A., Koziris, L.P., Mangino, L.C., Fry, A.C. and Newton R.U. 1996. "Influence of Compression Garments on Vertical Jump Performance in NCAA Division I Volleyball Players". Journal of Strength and Conditioning Research. Volume 10.3. Pages 180-183.

Kuethe, A.M. 1970. "Boundary Layer Control of Flow Separation and Heat Exchange". US Patent 3,741,285. U.S. Department of Commerce, Washington DC.

Kuethe, A.M. 1972. "Effect of Streamwise Vortices on Wake Properties Associated with Sound Generation". Journal of Aircraft. Volume 9. Pages 715-719.

Kuethe, A.M and Chow, C. 1986. *Foundations of Aerodynamics, Bases of Aerodynamic Design, Fourth Edition.* John Wiley & Sons, Inc., New York, NY.

Landolt, H. and Börnstein, R. 1955. *Values and Functions of Physics, Chemistry, Astronomy, Geophysics, and Technique.* Volume 4, Part 1. Springer-Verlag, Berlin.

Lin, J.C., Howard, F.G. and Selby, G.V. 1990. "Small Submerged Vortex Generators for Turbulent Flow Separation Control". Journal of Spacecraft and Rockets. Volume 27, Number 5. Pages 503-507.

Lipson, C. and Sheth, N.J. 1973. *Statistical Design and Analysis of Engineering Experiments.* McGraw-Hill, Inc., New York, NY.

McNeill, A.R. 1968. *Animal Mechanics.* Sandwich and Jackson, London.

Rao, D.M. and Kariya, T.T. 1988. "Boundary-Layer Submerged Vortex Generators for Separation Control – An Experimental Study". American Institute of Aeronautics and Astronautics. AIAA Paper 88-3546.

Rae, Jr.,W.H. and Pope, A. 1984. *Low-Speed Wind Tunnel Testing, Third Edition.* John Wiley & Sons, Inc., New York, NY.

RAS 66029. 1981. "Subsonic Performance Data for NACA Type Submerged Air Intakes". Royal Aeronautical Society.

Stephens, A.V. 1957. "Solid Boundary Surface for Contact with a Relatively Moving Fluid Medium". U.S. Patent No. 2,800,291. U.S. Department of Commerce, Washington DC.

Tietjens, O.G. 1957. *Applied Hydro- and Aerodynamics.* Dover Books, New York, NY.

Toussaint, H.M., Hollander, A.P., de Groot, G., van Ingen Schenau, G., Vervoorn, K., de Best, H., Meulemans, T. and Schreurs, W. 1988. "Measurement of Efficiency in Swimming Man". 5th International Symposium of Biomechanics and Medicine in Swimming. Pages 45-52.

Waring, J.C.S. 1998. "Wearable Article for Athlete with Vortex Generators to Reduce Form Drag". U.S. Patent No. 5,734,990. U.S. Department of Commerce, Washington DC.

Walsh, M.J. 1980. "Viscous Drag Reduction". Progress in Astronautics and Aeronautics. Volume 72.

Wheeler, G.O. 1984. "Means of Maintaining Attached Flow of a Flow Medium". U.S. Patent No. 4,455,045. U.S. Department of Commerce, Washington DC.

Wheeler, G.O. 1991. "Low Drag Vortex Generators". U.S. Patent No. 5,058,837. U.S. Department of Commerce, Washington DC.

White, F.M. 1979. *Fluid Mechanics*. McGraw-Hill, Inc., New York, NY.

White, F.M. 1991. *Viscous Fluid Flow, Second Edition*. McGraw-Hill, Inc., New York, NY.

Wyse, E. 1997. *The Guinness Book of World Records*. Guiness Publishing Limited. Enfield, Middlesex, England.

Appendix A - Tare Drag Estimate

Any supporting structure exposed to wind in the test section will generate tare drag that must be subtracted from the measured drag. The tare drag is assumed to take the form

$$D_{tare} = C_{Dtare} A_{tare} \frac{1}{2} \rho V^2$$

since $\frac{1}{2} \rho V^2$ is the dynamic pressure that is measured for each data point, the quantity of interest is $C_{Dtare} A_{tare}$. This quantity is determined by adding the individual values of $C_D A$ for each item of support structure exposed to wind. The exposed cross-sectional area for each bayonet is

$$A_{bayonet} = 10in \cdot 0.1875in = 1.875in^2.$$

The profile of each bayonet is an elongated rectangle with slightly rounded corners. Its coefficient of drag is estimated to be

$$C_{Dbayonet} \approx 1.0.$$

Two bosses on either side of the model connect it to the bayonets. The exposed cross-sectional area of each boss is

$$A_{boss} = 0.85in \cdot 0.29in = 0.2465in^2$$

Each boss has an airfoil profile with a thickness-to-chord ratio of 46% and an aspect ratio of 1.36. This suggests a drag coefficient of

$$C_{Dboss} \approx 0.2.$$

Finally, the pitch strut has an exposed cross-sectional area of

$$A_{pstrut} = 7.5in \cdot .1875in = 1.4063in^2.$$

The pitch strut profile has thickness-to-chord ratio of 46% and an aspect ratio of 18.5. This suggests a drag coefficient of

$$C_{Dpstrut} \approx 0.1$$

The value of $C_{Dtare}A_{tare}$ is given by

$$C_{Dtare}A_{tare} = 2 \cdot C_{Dbayonet}A_{bayonet} + 2 \cdot C_{Dboss}A_{boss} + C_{Dpstrut}A_{pstrut}.$$

Substituting in the values from above gives

$$C_{Dtare}A_{tare} = 3.99in^2$$

This value was multiplied by the dynamic pressure measured for each data point and subtracted from the measured drag.

Appendix B - Test Data

Table 1: Test Data for Baseline Configuration with Fabric Strips

ID	Configuration	ρ	μ	q	V	Re	LogRe	D	C_D
		kg/m^2	kg/m/sec	Pa	m/sec	x 10^6		N	
1	Fabric Baseline	1.187	1.812E-05	546.2	30.33	2.483	6.395	5.91	0.558
2		1.187	1.812E-05	879.8	38.50	3.152	6.499	9.49	0.556
3		1.185	1.815E-05	1260.4	46.13	3.764	6.576	13.72	0.561
4		1.183	1.818E-05	1262.8	46.21	3.758	6.575	13.75	0.561
5		1.180	1.820E-05	1272.7	46.44	3.764	6.576	13.92	0.564
6		1.178	1.823E-05	1270.2	46.44	3.751	6.574	13.70	0.556
7		1.184	1.815E-05	543.7	30.31	2.471	6.393	5.95	0.564
8		1.182	1.818E-05	864.9	38.26	3.109	6.493	9.36	0.558
9		1.179	1.820E-05	1267.8	46.37	3.755	6.575	13.85	0.563
10		1.179	1.820E-05	548.6	30.50	2.470	6.393	6.01	0.565
11		1.177	1.823E-05	872.4	38.50	3.107	6.492	9.49	0.561
12		1.175	1.826E-05	1275.2	46.59	3.748	6.574	13.90	0.562
13		1.175	1.826E-05	542.4	30.39	2.444	6.388	5.98	0.568
14		1.173	1.828E-05	882.2	38.79	3.110	6.493	9.62	0.562
15		1.171	1.831E-05	1267.8	46.54	3.719	6.570	13.79	0.561

Table 2: Test Data for Clean Baseline Configuration

ID	Configuration	ρ	μ	q	V	Re	LogRe	D	C_D
		kg/m^2	kg/m/sec	Pa	m/sec	$x\ 10^6$		N	
16	Clean Baseline	1.180	1.812E-05	536.3	30.15	2.454	6.390	5.45	0.524
17		1.178	1.815E-05	864.9	38.32	3.109	6.493	8.60	0.513
18		1.176	1.818E-05	1265.3	46.39	3.751	6.574	12.51	0.510
19		1.163	1.834E-05	1245.5	46.29	3.668	6.564	12.38	0.512
20		1.161	1.836E-05	1259.1	46.58	3.680	6.566	12.48	0.511
21		1.158	1.839E-05	1257.9	46.60	3.669	6.565	12.47	0.511
22		1.182	1.818E-05	543.7	30.33	2.465	6.392	5.53	0.524
23		1.179	1.820E-05	871.1	38.43	3.113	6.493	8.77	0.519
24		1.177	1.823E-05	1282.6	46.68	3.768	6.576	12.69	0.510
25		1.195	1.807E-05	1267.8	46.06	3.808	6.581	12.62	0.513
26		1.193	1.810E-05	1252.9	45.84	3.776	6.577	12.49	0.514
27		1.191	1.812E-05	1257.9	45.97	3.775	6.577	12.58	0.515
28		1.166	1.818E-05	536.3	30.33	2.432	6.386	5.51	0.530
29		1.166	1.818E-05	871.1	38.65	3.100	6.491	8.83	0.522
30		1.164	1.820E-05	1277.7	46.86	3.745	6.573	12.73	0.514

Table 3: Test Data for Clean Baseline Configuration (Continued)

ID	Configuration	r	m	q	V	Re	LogRe	D	C_D
		kg/m^2	kg/m/sec	Pa	m/sec	x 10^6		N	
31	Clean Baseline	1.162	1.823E-05	1295.0	47.22	3.761	6.575	12.91	0.514
32	Continued	1.162	1.823E-05	1282.6	46.99	3.743	6.573	12.74	0.512
33		1.160	1.826E-05	1265.3	46.72	3.709	6.569	12.66	0.516
34		1.201	1.802E-05	595.6	31.50	2.624	6.419	6.00	0.519
35		1.201	1.802E-05	919.3	39.13	3.260	6.513	9.37	0.526
36		1.198	1.804E-05	1277.7	46.18	3.834	6.584	12.73	0.514
37		1.196	1.807E-05	1104.7	42.98	3.556	6.551	11.01	0.514
38		1.194	1.810E-05	729.0	34.95	2.882	6.460	7.37	0.521
39		1.196	1.807E-05	578.3	31.10	2.573	6.410	5.91	0.526
40		1.196	1.807E-05	741.4	35.21	2.913	6.464	7.48	0.520
41		1.194	1.810E-05	911.9	39.09	3.223	6.508	9.17	0.518
42		1.194	1.810E-05	1114.5	43.21	3.563	6.552	11.24	0.520
43		1.192	1.812E-05	1341.9	47.46	3.900	6.591	13.48	0.518
44		1.192	1.807E-05	551.1	30.41	2.507	6.399	5.54	0.518
45		1.192	1.807E-05	887.2	38.59	3.181	6.503	8.80	0.511
46		1.189	1.810E-05	1270.2	46.22	3.797	6.579	12.55	0.509

Table 4: Test Data for Fabric Mounted Stephens Configurations without Vortex Generators on Back and X = 1.25in

ID	VG Type	Mount	Configuration	ρ	μ	q	V	Re	LogRe	D	C_D
			R3	kg/m^2	kg/m/s	Pa	m/sec			N	
					$x\ 10^{-5}$			$x\ 10^{6}$			
47	Stephens	Fabric	20-0-0-0-0-1.25-0	1.192	1.820	561.0	30.69	2.511	6.400	5.82	0.535
48				1.192	1.823	894.6	38.75	3.167	6.501	9.19	0.530
49				1.189	1.825	1287.5	46.53	3.790	6.579	13.11	0.525
50				1.187	1.828	546.2	30.33	2.462	6.391	5.67	0.535
51				1.187	1.828	867.4	38.23	3.103	6.492	8.93	0.531
52				1.185	1.831	1270.2	46.31	3.746	6.574	13.00	0.528
53				1.183	1.833	551.1	30.53	2.461	6.391	5.79	0.541
54				1.183	1.833	874.8	38.46	3.101	6.492	9.03	0.532
55				1.180	1.836	1277.7	46.53	3.739	6.573	12.98	0.524
56	Stephens	Fabric	20-12-0-0-0-1.25-0	1.187	1.828	536.3	30.06	2.440	6.387	5.69	0.547
57				1.187	1.828	874.8	38.39	3.116	6.494	9.23	0.544
58				1.185	1.831	1285.1	46.58	3.768	6.576	13.41	0.538
59				1.183	1.833	528.9	29.91	2.411	6.382	5.71	0.556
60				1.183	1.833	887.2	38.74	3.123	6.495	9.33	0.542
61				1.180	1.836	1265.3	46.30	3.721	6.571	13.17	0.537
62				1.178	1.839	541.2	30.31	2.427	6.385	5.77	0.549
63				1.178	1.839	872.4	38.48	3.082	6.489	9.22	0.545
64				1.176	1.842	1267.8	46.43	3.706	6.569	13.26	0.539

Table 5: Test Data for Fabric Mounted Stephens Configurations with Vortex Generators on Back and X = 1.25in

ID	VG Type	Mount	Configuration	ρ	μ	q	V	Re	LogRe	D	C_D
			R3	kg/m^2	kg/m/s	Pa	m/sec			N	
					$\times 10^{-5}$			$\times 10^6$			
65	Stephens	Fabric	20-12-0-10-12-1.25-9	1.187	1.828	548.6	30.40	2.468	6.392	5.88	0.552
66				1.187	1.828	874.8	38.39	3.116	6.494	9.36	0.551
67				1.185	1.831	1267.8	46.26	3.742	6.573	13.37	0.544
68				1.183	1.833	543.7	30.32	2.445	6.388	5.78	0.548
69				1.183	1.833	879.8	38.57	3.110	6.493	9.31	0.546
70				1.180	1.836	1265.3	46.30	3.721	6.571	13.34	0.544
71				1.178	1.839	548.6	30.52	2.444	6.388	5.82	0.547
72				1.178	1.839	877.3	38.59	3.091	6.490	9.36	0.550
73				1.176	1.842	1267.8	46.43	3.706	6.569	13.41	0.545
74	Stephens	Fabric	20-12-0-10-12-1.25-7	1.187	1.828	548.6	30.40	2.468	6.392	5.83	0.548
75				1.187	1.828	869.9	38.28	3.107	6.492	9.20	0.545
76				1.185	1.831	1260.4	46.13	3.731	6.572	13.19	0.539
77				1.183	1.833	551.1	30.53	2.461	6.391	5.92	0.554
78				1.183	1.833	872.4	38.41	3.097	6.491	9.27	0.548
79				1.180	1.836	1265.3	46.30	3.721	6.571	13.26	0.540
80				1.178	1.839	546.2	30.45	2.439	6.387	5.84	0.551
81				1.178	1.839	872.4	38.48	3.082	6.489	9.27	0.548
82				1.176	1.842	1260.4	46.30	3.696	6.568	13.20	0.540

Table 6: Test Data for Fabric Mounted Stephens Configurations with Vortex Generators on Back and X = 1.25in (Continued)

ID	VG Type	Mount	Configuration	ρ	μ	q	V	Re	LogRe	D	C_D
			R3	kg/m^2	kg/m/s	Pa	m/sec			N	
					$\times 10^{-5}$			$\times 10^{6}$			
83	Stephens	Fabric	20-12-0-1-12-1.25-9	1.187	1.828	548.6	30.40	2.468	6.392	5.84	0.549
84				1.187	1.828	877.3	38.45	3.121	6.494	9.41	0.553
85				1.185	1.831	1265.3	46.22	3.739	6.573	13.33	0.543
86				1.183	1.833	548.6	30.46	2.456	6.390	5.90	0.554
87				1.183	1.833	882.2	38.63	3.114	6.493	9.48	0.554
88				1.180	1.836	1262.8	46.26	3.717	6.570	13.30	0.543
89				1.178	1.839	538.7	30.24	2.422	6.384	5.82	0.557
90				1.178	1.839	864.9	38.32	3.069	6.487	9.22	0.549
91				1.176	1.842	1262.8	46.34	3.699	6.568	13.33	0.544
92	Stephens	Fabric	20-12-0-1-1-1.25-9	1.187	1.828	536.3	30.06	2.440	6.387	5.78	0.556
93				1.187	1.828	869.9	38.28	3.107	6.492	9.23	0.547
94				1.185	1.831	1252.9	45.99	3.720	6.571	13.24	0.545

Table 7: Test Data for Fabric Mounted Stephens Configurations without Vortex Generators on Back and X = 0.75in

ID	VG Type	Mount	Configuration	ρ	μ	q	V	Re	LogRe	D	C_D
			R3	kg/m^2	kg/m/s	Pa	m/sec			N	
					$\times 10^{-5}$			$\times 10^{6}$			
95	Stephens	Fabric	14-12-0-0-0-0.75-0	1.182	1.833	542.4	30.30	2.441	6.388	5.81	0.552
96				1.179	1.836	889.7	38.84	3.119	6.494	9.16	0.531
97				1.177	1.839	1275.2	46.54	3.725	6.571	13.02	0.526
98				1.177	1.839	543.7	30.39	2.432	6.386	5.80	0.550
99				1.175	1.842	869.9	38.48	3.069	6.487	8.97	0.532
100				1.173	1.844	1280.1	46.72	3.714	6.570	13.07	0.526
101				1.173	1.844	548.6	30.59	2.431	6.386	5.83	0.548
102				1.171	1.847	879.8	38.77	3.072	6.487	9.16	0.536
103				1.169	1.850	1292.5	47.03	3.714	6.570	13.30	0.530

Table 8: Test Data for Directly Mounted Stephens Configurations with X = 1.25in

ID	VG Type	Mount	Configuration	ρ	μ	q	V	Re	LogRe	D	C_D
			R3	kg/m^2	kg/m/s	Pa	m/sec			N	
					$\times 10^{-5}$			$\times 10^{6}$			
104	Stephens	Direct	18-0-0-0-0-1.25-0	1.183	1.828	872.4	38.41	3.106	6.492	8.89	0.525
105				1.180	1.831	867.4	38.34	3.090	6.490	8.81	0.523
106				1.180	1.831	872.4	38.44	3.099	6.491	8.85	0.523
107				1.183	1.828	857.5	38.08	3.080	6.488	8.64	0.519
108				1.180	1.831	860.0	38.17	3.077	6.488	8.67	0.519
109				1.180	1.831	857.5	38.12	3.072	6.487	8.69	0.523
110	Stephens	Direct	18-14-0-0-0-1.25-0	1.183	1.828	864.9	38.24	3.093	6.490	8.73	0.520
111				1.180	1.831	862.5	38.23	3.081	6.489	8.69	0.519
112				1.180	1.831	869.9	38.39	3.094	6.491	8.87	0.526
113				1.183	1.828	887.2	38.73	3.132	6.496	9.05	0.526
114				1.180	1.831	855.1	38.06	3.068	6.487	8.75	0.528
115				1.180	1.831	857.5	38.12	3.072	6.487	8.79	0.528
116	Stephens	Direct	18-14-8-0-0-1.25-0	1.183	1.828	845.2	37.80	3.057	6.485	9.08	0.554

Table 9: Test Data for Directly Mounted Stephens Configurations with X = 0.75in

ID	VG Type	Mount	Configuration	ρ	μ	q	V	Re	LogRe	D	C_D
			R3	kg/m^2	kg/m/s	Pa	m/sec			N	
					$\times 10^{-5}$			$\times 10^{6}$			
117	Stephens	Direct	16-0-0-0-0-0.75-0	1.200	1.814	862.5	37.91	3.134	6.496	8.75	0.523
118				1.198	1.817	869.9	38.11	3.140	6.497	8.81	0.522
119				1.198	1.817	872.4	38.16	3.145	6.498	8.87	0.524
120	Stephens	Direct	16-14-0-0-0-0.75-0	1.196	1.820	867.4	38.09	3.128	6.495	9.02	0.536
121				1.193	1.823	543.7	30.19	2.470	6.393	5.74	0.544
122				1.191	1.825	1270.2	46.18	3.767	6.576	13.05	0.529
123	Stephens	Direct	0-14-0-0-0-0.75-0	1.191	1.825	538.7	30.08	2.453	6.390	5.61	0.536
124				1.191	1.823	877.3	38.39	3.135	6.496	9.06	0.532
125				1.188	1.825	1262.8	46.10	3.752	6.574	13.22	0.540
126	Stephens	Direct	8-14-0-0-0-0.75-0	1.188	1.825	543.7	30.25	2.462	6.391	5.67	0.537
127				1.186	1.828	864.9	38.19	3.097	6.491	8.87	0.529
128				1.184	1.831	1314.7	47.13	3.809	6.581	13.38	0.524
129	Stephens	Direct	8-3-0-0-0-0.75-0	1.188	1.825	544.9	30.28	2.464	6.392	5.53	0.523
130				1.186	1.828	877.3	38.46	3.119	6.494	8.82	0.518
131				1.184	1.831	1265.3	46.23	3.737	6.573	12.56	0.512

Table 10: Test Data for Directly Mounted Stephens Configurations with X = 0.75in (Continued)

ID	VG Type	Mount	Configuration	ρ	μ	q	V	Re	LogRe	D	C_D
			R3	kg/m^2	kg/m/s	Pa	m/sec			N	
					x 10^{-5}			x 10^6			
132	Stephens	Direct	8-4-0-0-0-0.75-0	1.188	1.825	546.2	30.32	2.467	6.392	5.62	0.530
133				1.186	1.828	871.1	38.33	3.108	6.493	8.74	0.517
134				1.184	1.831	1267.8	46.28	3.741	6.573	12.58	0.511
135	Stephens	Direct	11-7-0-0-0-0.75-0	1.184	1.831	548.6	30.44	2.461	6.391	5.71	0.536
136				1.182	1.833	879.8	38.59	3.109	6.493	8.97	0.525
137	Stephens	Direct	10-7-0-0-0-0.75-0	1.186	1.828	546.2	30.35	2.461	6.391	5.70	0.538
138				1.184	1.831	872.4	38.39	3.103	6.492	8.93	0.528
139				1.182	1.833	1275.2	46.46	3.743	6.573	12.83	0.519
140	Stephens	Direct	12-4-0-0-0-0.75-0	1.186	1.828	536.3	30.07	2.439	6.387	5.54	0.532
141				1.184	1.831	867.4	38.28	3.094	6.491	8.77	0.521
142				1.182	1.833	1267.8	46.32	3.732	6.572	12.74	0.518
143	Stephens	Direct	14-12-0-0-0-0.75-0	1.186	1.828	548.6	30.42	2.467	6.392	5.72	0.537
144				1.184	1.831	866.2	38.25	3.092	6.490	8.93	0.531
145				1.182	1.833	1280.1	46.55	3.750	6.574	13.06	0.526
146	Stephens	Direct	14-12-0-1-0-0.75-9	1.184	1.831	549.9	30.48	2.464	6.392	5.82	0.546
147				1.182	1.833	871.1	38.40	3.093	6.490	9.09	0.538
148				1.179	1.836	1277.7	46.55	3.737	6.573	13.17	0.532

Table 11: Test Data for Kuethe Type 1 Vortex Generators

ID	VG Type	Mount	Configuration	ρ	μ	q	V	Re	LogRe	D	C_D
			R3	kg/m^2	kg/m/s	Pa	m/sec			N	
					x 10^{-5}			x 10^6			
149	Kuethe T1	Direct	31-0-0-0-0-0.75-0	1.178	1.831	541.2	30.31	2.438	6.387	5.37	0.512
150				1.176	1.833	869.9	38.47	3.083	6.489	8.60	0.510
151				1.174	1.836	1267.8	46.48	3.713	6.570	12.62	0.513
152	Kuethe T1	Direct	31-17-0-0-0-0.75-0	1.174	1.836	541.2	30.37	2.426	6.385	5.45	0.519
153				1.171	1.839	879.8	38.76	3.086	6.489	8.66	0.507
154				1.169	1.842	1262.8	46.48	3.688	6.567	12.21	0.498
155				1.167	1.844	1270.2	46.66	3.690	6.567	12.29	0.499
156				1.165	1.847	1267.8	46.66	3.678	6.566	12.25	0.498
157				1.163	1.850	1259.1	46.54	3.657	6.563	12.15	0.498

Table 12: Test Data for Kuethe Type 2 Vortex Generators

ID	VG Type	Mount	Configuration	ρ	μ	q	V	Re	LogRe	D	C_D
			R3	kg/m^2	kg/m/s	Pa	m/sec			N	
					$\times 10^{-5}$			$\times 10^{6}$			
158	Kuethe T2	Direct	10-8-0-0-0-0.75-0	1.170	1.828	531.3	30.13	2.412	6.382	5.49	0.532
159				1.170	1.828	869.9	38.55	3.086	6.489	8.63	0.511
160				1.168	1.831	1267.8	46.59	3.716	6.570	12.39	0.504
161				1.166	1.833	528.9	30.12	2.394	6.379	5.43	0.529
162				1.166	1.833	877.3	38.79	3.084	6.489	8.70	0.511
163				1.164	1.836	1275.2	46.81	3.709	6.569	12.49	0.505
164				1.162	1.839	541.2	30.52	2.410	6.382	5.51	0.525
165				1.162	1.839	892.1	39.19	3.095	6.491	8.82	0.509
166				1.164	1.836	528.9	30.15	2.389	6.378	5.45	0.531
167				1.164	1.836	866.2	38.58	3.057	6.485	8.61	0.513
168	Kuethe T2	Direct	10-8-0-0-0-1.0-0	1.166	1.833	540.0	30.43	2.419	6.384	5.58	0.533
169				1.166	1.833	866.2	38.54	3.064	6.486	8.68	0.517
170				1.164	1.836	1270.2	46.72	3.702	6.568	12.63	0.513
171	Kuethe T2	Direct	10-0-0-0-0-1.0-0	1.166	1.833	541.2	30.47	2.422	6.384	5.48	0.522
172				1.166	1.833	872.4	38.68	3.075	6.488	8.72	0.515
173				1.164	1.836	1275.2	46.81	3.709	6.569	12.62	0.510
174	Kuethe T2	Direct	10-0-0-0-0-0.75-0	1.164	1.836	541.2	30.50	2.416	6.383	5.51	0.525
175				1.164	1.836	869.9	38.66	3.063	6.486	8.74	0.518
176				1.162	1.839	1260.4	46.58	3.678	6.566	12.46	0.509